The artemisinin-induced dormant stages of *Plasmodium falciparum* exhibit hallmarks of cellular quiescence/senescence and drug resilience

Check for updates

Jaishree Tripathi [1,2,6] ✉, Michal Stoklasa[1,6], Sourav Nayak[1], Kay En Low[3], Erica Qian Hui Lee[2], Quang Huy Duong Tien [1], Laurent Rénia[1,4,5], Benoit Malleret [2,3] & Zbynek Bozdech [1] ✉

Recrudescent infections with the human malaria parasite, *Plasmodium falciparum*, presented traditionally the major setback of artemisinin-based monotherapies. Although the introduction of artemisinin combination therapies (ACT) largely solved the problem, the ability of artemisinin to induce dormant parasites still poses an obstacle for current as well as future malaria chemotherapeutics. Here, we use a laboratory model for induction of dormant *P. falciparum* parasites and characterize their transcriptome, drug sensitivity profile, and cellular ultrastructure. We show that *P. falciparum* dormancy requires a ~5-day maturation process during which the genome-wide gene expression pattern gradually transitions from the ring-like state to a unique form. The transcriptome of the mature dormant stage carries hallmarks of both cellular quiescence and senescence, with downregulation of most cellular functions associated with growth and development and upregulation of selected metabolic functions and DNA repair. Moreover, the *P. falciparum* dormant stage is considerably more resistant to antimalaria drugs compared to the fast-growing asexual stages. Finally, the irregular cellular ultrastructure further suggests unique properties of this developmental stage of the *P. falciparum* life cycle that should be taken into consideration by malaria control strategies.

Artemisinin combination therapy (ACT) is currently the backbone of all malaria elimination programs around the world[1]. Since their implementation in the early 2000s, ACTs have contributed considerably to the reduction of malaria morbidity and mortality achieved in the first two decades of the 21st century worldwide. Unfortunately, the decreasing efficacy of ACT emerged in the eastern part of the Greater Mekong Subregion as early as 2009[2,3] and is now emerging in other parts of the world, including sub-Saharan Africa[4–6], which is posing a

[1]School of Biological Sciences, Nanyang Technological University (NTU), Singapore 637551, Singapore. [2]Department of Microbiology and Immunology, Immunology Translational Research Programme, Yong Loo Lin School of Medicine, National University of Singapore (NUS), Singapore 117597, Singapore. [3]Electron Microscopy Unit, Yong Loo Lin School of Medicine, National University of Singapore (NUS), Singapore 117597, Singapore. [4]Lee Kong Chian School of Medicine, Nanyang Technological University (NTU), Singapore 636921, Singapore. [5]A*STAR Infectious Diseases Labs (A*STAR ID Labs), Agency for Science, Technology and Research (A*STAR), Singapore 138648, Singapore. [6]These authors contributed equally: Jaishree Tripathi, Michal Stoklasa. ✉e-mail: jtmic@nus.edu.sg; zbozdech@ntu.edu.sg

major concern for the future[7,8]. Better understanding of the ACT mode(s) of action and their resistance mechanisms is still urgently needed for managing their current clinical implementations and rational designs of new strategies[9].

All currently used ACTs are composed of two main components: (i.) fast-acting artemisinin or its derivatives (further artemisinins), mediating the removal of the majority of the parasites during the early stages of the treatment course; (ii.) the long-lasting/acting partner drugs that eliminate the residual parasite loads remaining in the patient during the later stages of the treatment[10]. The rationale for this ACT design is based on the short bioavailability of artemisinin that, despite its high antiparasitic potency, often fails to eliminate all infected erythrocytes[11,12]. Indeed, in earlier clinical monotherapy-based implementations, artemisinins were highly effective in rapidly reducing parasite loads in uncomplicated *P. falciparum* infections, yielding complete parasite clearance after a 5 to 7-day treatment period (reviewed in ref. 13). Despite this, considerable recrudescence was reported essentially in all the clinical studies with a wide range of occurrence (3–50%)[14], depending on geographical and epidemiological background. Interestingly, the rate of recrudescence appears to be linked predominantly with the overall parasite load at the start of the treatment rather than other epidemiological or clinical factors[14]. This indicated that the recrudescing infections rise from (some form of) a residual parasite fraction that remains in the patient's body after the 5–7-day treatment. It is plausible that this "residual" parasite population consists of unique parasite forms that are resilient to further artemisinin treatment and can persist in the patient's body for extended periods. The most fitting hypothesis for such parasite form is a dormant state that was previously observed in other microbial pathogens such as bacteria[15] although additional and nonexclusive explanations such as increased immune escape may also explain this phenomenon[16].

Indeed, exposure of *P. falciparum* to artemisinins in vitro induces dormancy-like forms that could represent this residual parasite (sub) population[17]. Initially reported by Kyle and Webster in 1996, treatment of the ring stage *P. falciparum* parasites with clinically relevant concentrations of artemisinins induced dormant parasites that can be detected as pyknotic-like cellular forms in an in vitro culture for 3–8 days[18]. Exploring this further, the same group established a tractable laboratory model in which treatment of ring stages with 700 nM (~ 200 ng/ml) of dihydroartemisinin (DHA) for 6 h (hr) drives parasites to dormancy that persists in an in vitro culture for up to 20 days[19]. In the following series of studies, it was shown that varying levels of drug resistance can affect the rate of dormancy-dependent recrudescence[20]. The persister parasites exhibit an altered pattern of development[21], expressing several genes related to metabolism[22] and cell cycle regulation[23].

Moreover, the dormant parasites are characterized by condensed cytoplasm and nucleus but enlarged mitochondrion that retains its membrane potential[24,25]. Indeed, there is a distinct rearrangement of the dormant parasite cellular structure with distinct, new mitochondrial-nuclear associations[25]. This restructuring is likely induced by oxidative stress and may lead to an altered transcriptional activity within the nucleus. In addition to the in vitro observation, there is now mounting evidence that dormant parasites also occur in vivo. Initially, pyknotic forms were shown to be induced by artemisinin in the in vivo rodent malaria model *P. vinckei*[26] but were also clearly detected in the blood of volunteers in control human infection studies infected with wild-type and PfK13 mutant/artemisinin resistant *P. falciparum* strains[27].

Taken together, these results suggest that persister forms of *P. falciparum* parasites could provide the reservoir for recrudescent infection after artemisinin monotherapy and, as such, play a role in the current ACT failures (*see above*). Here, we characterized the transcriptome of the artemisinin-induced dormant stage of *P. falciparum*, showing its highly unique composition carrying features of both cellular quiescence and senescence. We also demonstrate that the induced dormant forms require ~5 days of maturation, after which the resulting *day 5 mature dormant persisters* (d5MDP) exhibit resilience to a broad spectrum of antimalaria drugs persisting in a highly irregular cellular ultrastructure. The uncovered cellular and molecular features of the d5MDPs are consistent with their role as a residual parasite population responsible for recrudescence.

Results

Time course of the artemisinin-induced *P. falciparum* dormancy
To gain further insights into the biological processes that drive the induction and persistence of the dormant forms of *P. falciparum* parasites and the subsequent re-emergence of asexual intraerythrocytic growth, we adopted the culturing protocol originally developed by Teuscher, F. et. al.[19] with few modifications. Briefly, *P. falciparum* (3D7 strain) parasites, cultured in RPMI media supplemented with lipid-rich bovine serum albumin (Albumax) at 2% hematocrit at 8% parasitemia were synchronized at the ring stage (6–12 h post invasion, HPI) followed by exposure to 700 nM dihydroartemisinin (DHA) for 6 h. Subsequently, the cells were maintained in the culture for 12 days, conducting magnetic-assisted cell sorting (MACS) removal of mature asexual stages of the intraerythrocytic developmental cycle (IDC) each day for the first three days. The distribution of morphological stages and parasitemia was evaluated by microscopy (Giemsa-stained blood smear) and Fluorescence-Assisted Cell Sorting (FACS) (Fig. 1A–D; Figs. S1, S2A and S2B, also see Methods).

Using the Giemsa-stained blood smears, we observed that the overall parasitemia was maintained five days past the DHA treatment (Fig. S1A and Supplementary Data 1). However, even one day after the treatment (Day 1), most of the parasites (81.8%, average of four biological replicates, Fig. 1A) exhibited a condensed morphology, characterized by densely stained, small, round-shaped cells (Fig. 1B). This condensed parasite morphology contrasts the (initial) ring stages that are characterized by the "classical" O-ring shape representing the expanded, blue-stained cytoplasm along with a single dense formation along the periphery, representing the red/purple stained nucleus (Fig. 1B, Figs. S2A and S2B). The morphological transformation from ring to condensed forms after exposure to DHA is analogous to several previous studies that reported the formation of rounded morphology with blue-stained cytoplasm and red-stained chromatin in Giemsa smears of dormant parasites[19,20]. In our experimental setup, the proportion of the condensed parasite forms remained high in at least four independent experiments (>95%; also estimated by two independent microscopists) between Day 2 and Day 5. High proportions of the condensed parasite forms prevailed until Day 7 with minimal occurrence of asexual stages even though the magnetic-assisted removal of these stages was discontinued on Day 3. This indicates that during this section of the experiment (Day 3 to Day 7), the vast majority of the parasite culture remained dormant, exhibiting minimal to no multiplication (Fig. 1A and Fig. S1B). Past Day 7, we began to detect a higher proportion of asexually multiplying parasites which indicates the re-emergence of the asexual growth that is particularly evident on Day 10 when 60.2 % (average of four biological replicates) of the total parasitemia was represented by the asexual IDC forms (Fig. 1A). This temporal distribution of parasite morphological states across the 12-day time courses was reproduced four times, each time with highly similar counts (Fig. 1A and Fig. S1B, error bars). To complement the Giemsa-stained blood smears, we also carried out FACS-based analysis of the parasite cultures using Hoechst-Dihydroethidium (Hoechst-DHE) double-staining protocol[28], which can distinguish between the key IDC stages (rings, trophozoites and schizonts) (Fig. 1B, D, Fig. S1C). Here, the condensed parasite forms and ring stage parasites exhibited an identical fluorescence intensity and hence fell within the same gate (Fig. 1B, D, Fig. S1C). The parasite staging by FACS (Fig. 1D, Fig. S1C) closely mirrored the parasite counting by Giemsa staining (Fig. 1A) with
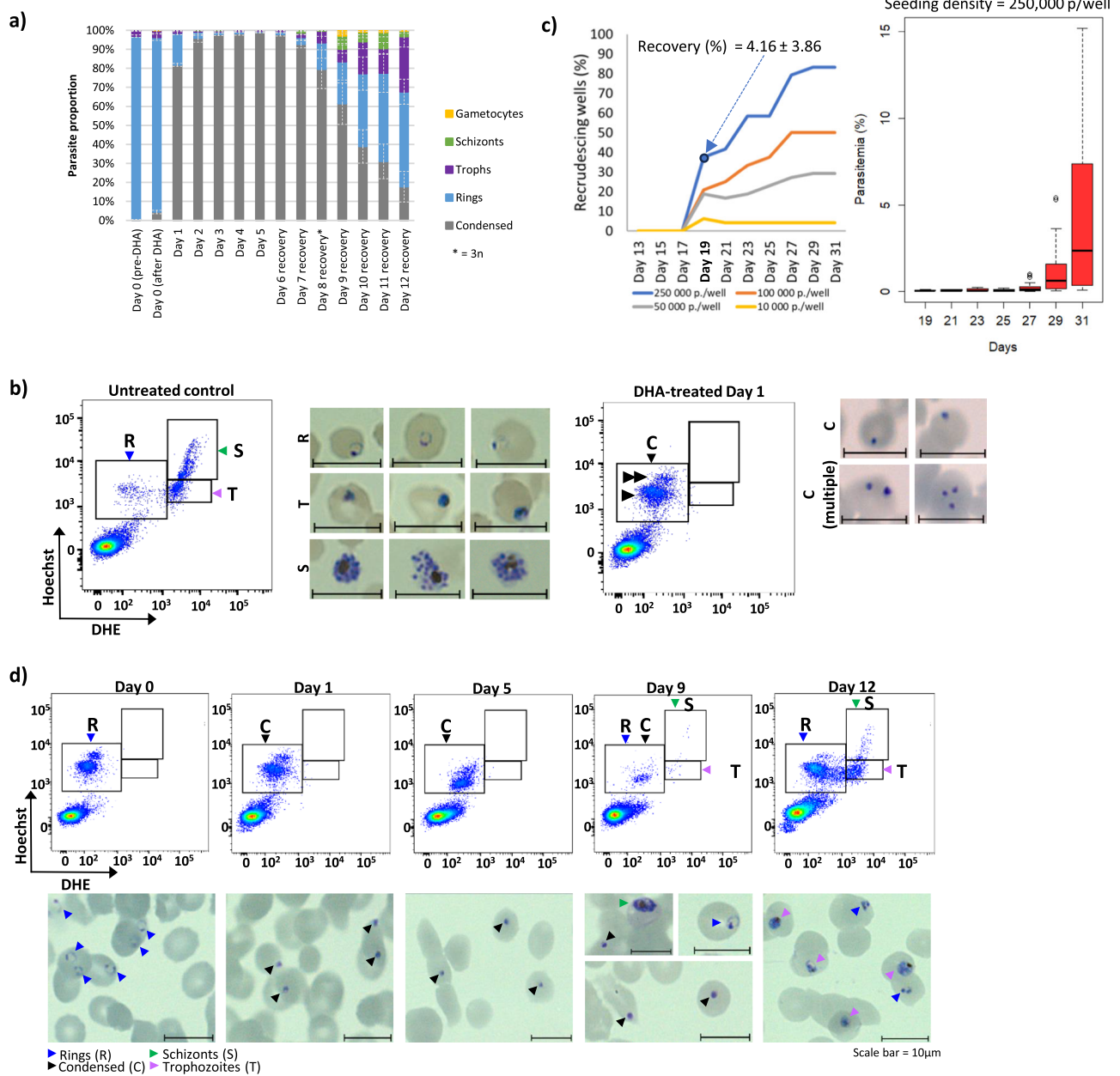
Fig. 1 | Dihydroartemisinin (DHA) Induced Dormant Stages of *P. falciparum* Parasites. a A bar graph showing stage proportions determined through microscopy of Giemsa-stained blood smears where 300 cells were counted for each day in four independent biological replicates unless stated otherwise. Error bars represent SEM. **b** A flow cytometry dot plot showing the gating strategy and sorting of parasites via FACS. An untreated control culture (left panel) with mixed IDC stages is shown in comparison to the DHA-treated culture on Day 1 (right panel). For distinguishing various *P. falciparum* stages, Hoechst 33342 and DHE staining were performed. To confirm the correct gating of different morphological stages, 3000-5000 infected RBCs were sorted into RPMI media and diluted into 0.3-0.5% parasitemia for the Giemsa smears shown here (see Methods). R rings, T trophozoite, S schizonts, C Condensed, single arrow infected RBCs with single condensed form parasites, double arrow infected RBCs with multiple condensed form parasites. Scale bar = 10 μm. This experiment was performed four times independently. **c** A line graph showing the number of recrudescent wells from Day 17 onwards. d5MDP

were seeded at 4 different densities (24 wells seeded each for 250 K and 100 K parasites per well; 48 wells seeded each for 50 K and 10 K parasites per well). Boxplot represents parasitemia measured between Day 19 to Day 31 by flow cytometry for recrudescing wells (250 K parasites per well). Each box represents the data from first to third quartile with the black horizontal line across each box representing the median. The top and bottom whiskers represent the maximum and minimum values of parasitemia (within the 1.5 times interquartile range) respectively. **d** Gating and sorting strategy for monitoring of the parasite's dormant stages induction and recovery process. The FACS plots shown represent DHE + Hoechst 33342 staining of synchronized parasite culture after excluding debris and doublets. Giemsa smears of the representative parasitic stages in culture on corresponding days are shown below the FACS plots with colored arrows pointing to the different parasite stages. Scale bar = 10 μm. This experiment was performed four times independently. Source data are provided as a Source Data file.

most of the parasites falling in the condensed forms-ring gate from Day 1 to Day 7 and full growth recovery observed from Day 10 onwards (Fig. S1C). The purity of each parasite stage isolated from various FACS gates was confirmed by Giemsa staining of the FACS sorted fraction (Fig. S1D).

The asexual growth recovery on Day 10–12 is likely a result of the revival of the dormant (condensed form) parasites but also the multiplication of the residual asexual forms remaining throughout the experimental course (albeit at low levels, Fig. 1A). The rapid rise in the proportion of asexual stages from Day 8 (~20%) to Day 10 (~60%)

suggests a considerable contribution of the dormancy recovery to this growth. This is particularly feasible given that the proportion of the residual asexual parasite was consistently low between Day 3 and Day 7, indicating minimal-to-no asexual multiplication during that period. To assess the propensity of the condensed parasite forms to give rise to asexual growth, we carried out an independent limited dilution experiment (Fig. 1C). Here, the DHA-induced *P. falciparum* condensed forms were seeded at increasing concentrations from 10,000 to 250,000 parasites per well ($n = 24$ or 48, Table S1). Parasite replication was monitored for 31 days via flow cytometry, and positive growth recovery was classified as when the overall parasitemia started to rise consistently above 0.02%, and the proportion of the trophozoite and schizont stages (FACS Q2%) exceeded 20% (Fig. S3). We observed that the number of wells exhibiting parasite recrudescence was directly proportional to the initial seeding density, suggesting the apparent recovery rate is influenced by in vitro culture condition (e.g. cell density) (Fig. 1C, left panel). For the 250,000 seeded cell experiment, 36% (9 out of 24) exhibited robust asexual growth on day 19, the earliest experimental time point, with statistically significant parasitemia measurements (seven generations from seeding on day 5). Taking this earliest experimental point, the estimated number of asexually growing parasites corresponds to $4.16\% \pm 3.86\%$ of the original parasitemia. Given the lack of information on the asexual multiplication rate in these recovering asexual cultures, the exact recovery rate remains elusive. However, the dilution recovery rate dynamics resemble the previously reported estimates between 0.044% to 1.313% established by Teucher, F. et al.[19]. The high cell density in our initial bulk cultures (Fig. 1A) suggests that the growth recovery of the dormant parasites contributed considerably to the high asexual parasitemia (~60.2%) observed on Day 10.

Nevertheless, given that only a small proportion of the presumed dormant parasites give rise to asexual growth, the main question remains to be addressed: the overall viability of the condensed parasite forms generated by this culturing system. Indeed, the overall dynamics of the bulk culture seem to suggest that most of the dormant parasites in this experiment do not reflect cell death but are in some form of a viable status. First, we observed close to 100% ring-to-condensed form conversion rate estimated according to the previous studies[18,19] which was highly reproducible in multiple biological replicas of the 3D7 and three additional *P. falciparum* strains (Figs. S4A and S4B). This was followed by sustained high levels of overall parasitemia that remained constant throughout the entire time course, indicating a minimal cell loss (Figs. S1A and S4A). The exception was the W2 strain, which also exhibited ~100% conversion rate but progressively declining parasitemia over 3 days. This may suggest that the condensed form is overall viability depends on the parasite's genetic background (see below) and that dead parasites do not persist in an in vitro culture. *Second*, the dormancy-inducing effect of DHA is distinct from other drugs, such as chloroquine. Specifically, chloroquine treatment of 6–12 HPI rings (CQ, 250 nM ($10 \times IC_{50}$) for 24 h) led to rapid reduction in parasitemia over three days during which the parasites exhibited mixed parasite morphology with both condensed and irregular/blebbed forms (Fig. S4D, E). Even though these observations provide compelling evidence, in the remainder of this study, we address the viability of the DHA-induced condensed/dormant forms of *P. falciparum* by transcriptomics, fluorescence viability markers, and drug susceptibility assays.

Transcriptome profiling of *P. falciparum* condensed forms uncovers the day 5 mature dormant persisters (d5MDP)

To investigate their viability and overall biological significance, we proceeded to reconstruct the global transcriptome of the DHA-induced condensed parasite forms over the entire 12-day time course. For this, we used the above-mentioned FACS-based cell isolation strategy coupled with "few-cells" RNA sequencing that allows morphology/stage-associated transcriptomic analysis of a defined number of *P. falciparum* cells[29]. Briefly, a bulk of 500 parasite cells was captured from the condensed forms/ring stage FACS gate each day and subjected to SMARTseq2-based RNA sequencing for whole transcriptome profiling[30] (for more details, see Methods & Supplementary protocol). Due to the need for RBC supplementation on Day 5 (Fig. S1A), the transcriptomic time course experiments were conducted in three separate phases: *induction and maturation* (further only *maturation*) between Day 0 to Day 5; *persistence* between Day 6-7; *re-emergence* of asexual growth between Day 8 and Day 12. While the *induction* and *re-emergence* phase transcriptome analyses were carried out in a single time course, the *persistence* phase was conducted in a separate experiment.

In the *maturation* and *re-emergence* transcriptomic dataset, we detected between 2152 to 3086 genes expressed in at least 80% of the time points representing the gene expression profile in at least one of the three biological replicas. Subsequently, we applied Fourier transformation to the identified gene expression profiles to generate an overview of the global transcriptomic pattern of the presumed *maturation* and *re-emergence* phases. Using one of the biological replicates (BR_C) as an overview dataset, we identified at least 786 genes that exhibited gradual downregulation in their mRNA levels during the *maturation* phase, reaching their minimum expression between Day 3 and 5 (Fig. 2A, *green bar*). Crucially, most of these genes exhibited (re)induction from Day 8 onwards, reaching their original ring-specific levels by Day 12. On the other hand, 1218 genes exhibited a progressive increase in expression from Day 1 to Day 5, with their peak expression exceeding their initial (Day 0, rings) mRNA levels starting Day 3. Analogously, the mRNA abundance of these genes fell back to the initial (low) levels on Day 10 through 12 (Fig. 2A, *red bar*). These results illustrate a dynamic expression pattern of more than 2000 (~35%) *P. falciparum* genes throughout the 12-day time course after the DHA-induction of condensed forms. This pattern is particularly surprising during the *maturation* phase (Day1–5) where we observed only gradual transcriptional changes contrasting the morphological profile with essentially all parasites in the condensed state (Fig. 1B, D). This suggests that during the first 5 days, the DHA-induced condensed forms of *P. falciparum* undergo a developmental process where the initial ring-like transcriptional profile gradually transitions into a unique pattern (see below). Curiously, while the Day 1 (and to some degree Day 2) parasites still relate transcriptionally to the ring stage (Spearman's Rank Correlation Coefficient, SPCC ~0.7), the transcriptional profile of the condensed parasites from Day 3 through Day 8, exhibit no resemblance to any stage of the asexual[30] (SPCC ~0.3) and sexual (SPCC < 0.3) intraerythrocytic growth (Fig. 2C, Fig. S5). Principal component analysis further shows distinct clusters being formed by asexual, sexual, and DHA-induced dormant parasite transcriptomes (Fig. S6A), suggesting fundamental transcriptomic differences between these developmentally distinct stages. Crucially, this correlation pattern is well preserved in all three biological replicas of the *maturation* and *re-emergence* phases (Fig. S5A, B). This also applies to the transcriptome of the *persistence* phase between Day 5-7, which bears no resemblance to any IDC or gametocytogenesis-bound developmental stages as indicated by low SPCC values (Fig. 3A, C, Fig. S5C). Moreover, there is a remarkably high correlation between the corresponding transcriptomes across the three biological replicas across all three phases, suggesting the specificity and reproducibility of these presumably dormant parasite transcriptional characteristics (Fig. 3C, Fig. S6B). This suggests that the observed transcriptomic reshuffling may represent an orchestrated transcriptional program that is "hardwired" into the *P. falciparum* genome, giving rise to a new previously undefined developmental stage. The concept of gradual transition might also be partly true for the *re-emergence* phase (Day 9–12), however, the 500-cell samples collected during this phase contained a progressively increasing number of morphologically
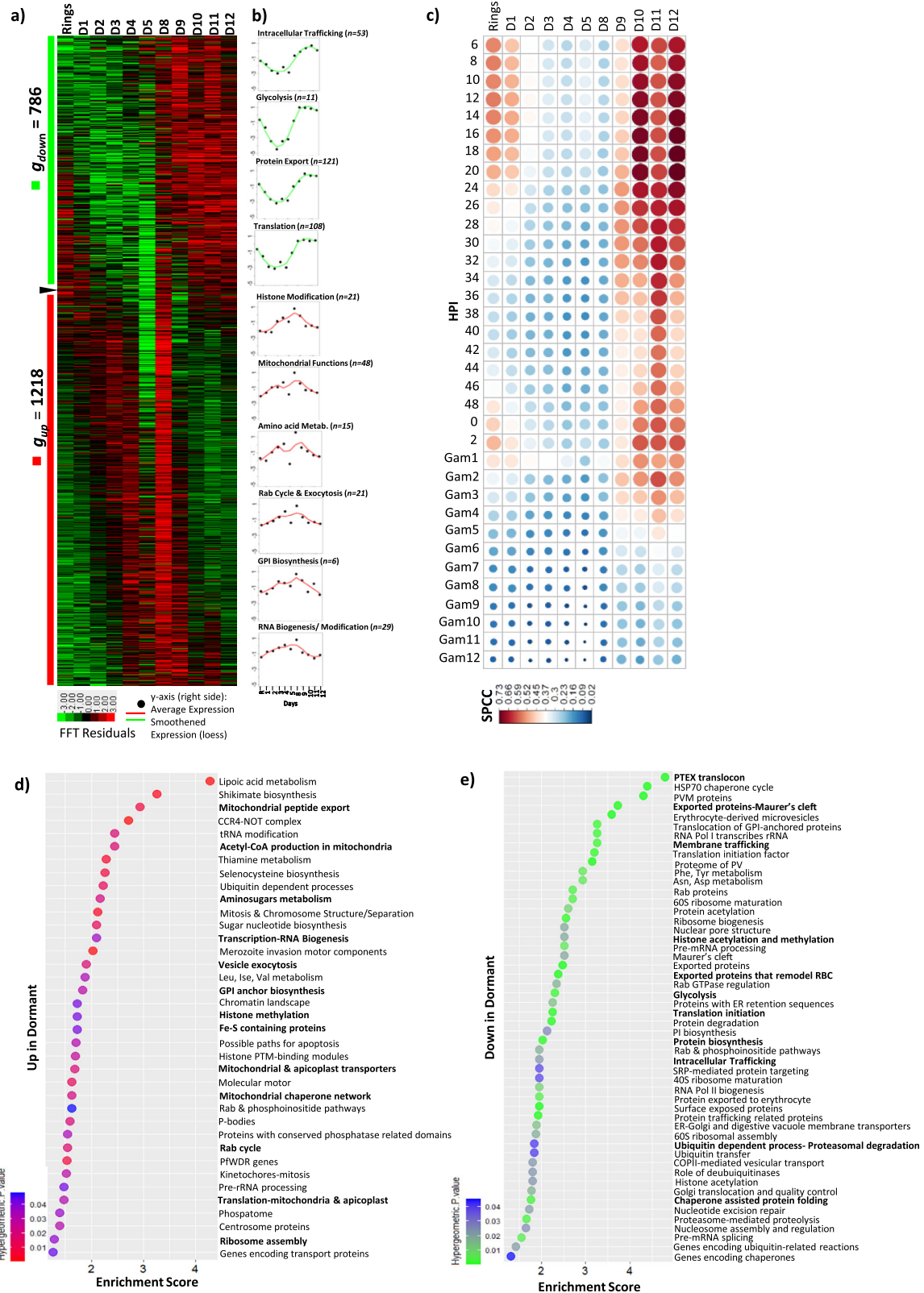
distinct rings masking the putative transcriptional profile of growth reemergence (Fig. 1A, D).

Taken together these data demonstrate that the DHA-induced dormant stages of *P. falciparum* represent a unique physiological state that requires 4-5 days for a maturation process represented by the gradual transcriptional transformations. For that reason, we wish to term the mature dormant stages the day five (5) Mature Dormant

Persister stage (d5MDP). The proposed concept of transcriptional retuning of the d5MDP is also supported by functional enrichment analyses that revealed their specific gene expression pattern with inductions/suppressions of several key metabolic and cellular functions. First, we observed a strong upregulation of a broad spectrum of genes involved in mitochondria-linked energy metabolism including ATP synthase subunits, cation-transporting ATPase 1,

Fig. 2 | Transcriptomic profiling of dormancy developmental cycle in DHA treated *P. falciparum*. a A heatmap depicting the Fourier-transformed gene expression profile of *P. falciparum* during the *induction* and *re-emergence* phase of DHA-induced dormancy (replicate BR_C). Genes upregulated and downregulated during Days 1 to 5 are highlighted by red bar (g_{up}) and green bar (g_{down}) respectively. **b** A line graph showing the average expression (smoothened) of key cellular pathways enriched amongst the upregulated (red) and downregulated (green) genes between Day 1 to 5. **c** A bubble plot depicting Pearson correlation coefficients (PCC) of *P. falciparum* transcriptomes obtained during the *induction-maturation* (Day 1 to 5) and *re-emergence* (Day 8 to 12) phases of dormancy in comparison to the high-resolution 3D7 reference transcriptomes for asexual (0-48 HPI) and sexual stages. **d**, **e** Bubble plots depicting pathways enriched amongst genes upregulated and downregulated during Day 1 to 5 after DHA induced pyknosis. All pathways are ordered by enrichment score and the color (red and green) denotes the statistical significance (hypergeometric *p*-value) in a one-sided hypergeometric test.

citrate/oxoglutarate carrier protein, cytosolic Fe-S cluster assembly factors and several mitochondrial and apicoplast ribosomal proteins during day 1 to day 5 (Fig. 2b). Additionally, several pathways linked to RNA biogenesis, GPI biosynthesis, histone modifications, mitosis and chromosome separation showed increased average expression during the dormancy *maturation* phase (Fig. 2b, lower panel). These are complemented by an array of specific cellular pathways such as mitochondrial peptide export, Acetyl-CoA production in mitochondria, amino-sugar metabolism, mitochondrial & apicoplast transporters, etc., all of which were found to be enriched amongst the genes induced during the d5MDP maturation (Fig. 2d). Inversely, glycolysis, factors of intracellular trafficking, protein export and translation were found to be suppressed through the d5MDP maturation (Fig. 2b, upper panel). This is specifically complemented by the suppression of factors involved in PTEX-complex, Mauer's Clefts, membrane trafficking, protein export to the host cell cytoplasm, and several amino acid biosynthesis pathways (Fig. 2e). The model of the specific metabolic and physiological state is also supported by the gene set enrichment analysis (GSEA) of the steady state transcriptome of the d5MDPs, reflecting the enrichment of cellular and metabolic pathways amongst genes with high mRNA levels (Fig. 3b). Essentially, genes involved in the formation of exosomes, centrosome, DNA repair machinery and nucleosome assembly exhibit the highest levels of expression in d5MDP, along with factors of mitochondrial DNA replication and cytochrome oxidase biogenesis and a specific subset of exported proteins. These functional representations of the transcriptional profiles were highly reproducible on the *maturation* and *persistence* phases of the d5MDPs, respectively (Fig. 3c, Figs. S7 and S8). By visual inspection of the fold-change and statistical significance (z-score) of the transcriptional changes, we identified several genes that could be used as transcriptomic markers differentiating between the rings and d5MDP. These include cytochrome c oxidase subunit 2 (PF3D7_1430900) and subunit 6B (PF3D7_0928000), ATP synthase F1 subunit (PF3D7_0217100), mitochondrial ribosomal protein S12 precursor, putative (PF3D7_0412100) and several spliceosomal RNA genes (e.g. PF3D7_1341100) upregulated in d5MDP (Supplementary Data 2). On the other hand, early transcribed membrane protein gene family members (e.g. PF3D7_0202500, PF3D7_1102800, PF3D7_1401400) and knob-associated histidine-rich protein (PF3D7_0202000) were upregulated in the ring stage parasites and massively downregulated in the d5MDPs. Next, we validated this differential expression and proposed that this panel of transcriptional markers could detect dormant parasites in various conditions using RNA-based quantitative RT-PCR (Fig. 3d).

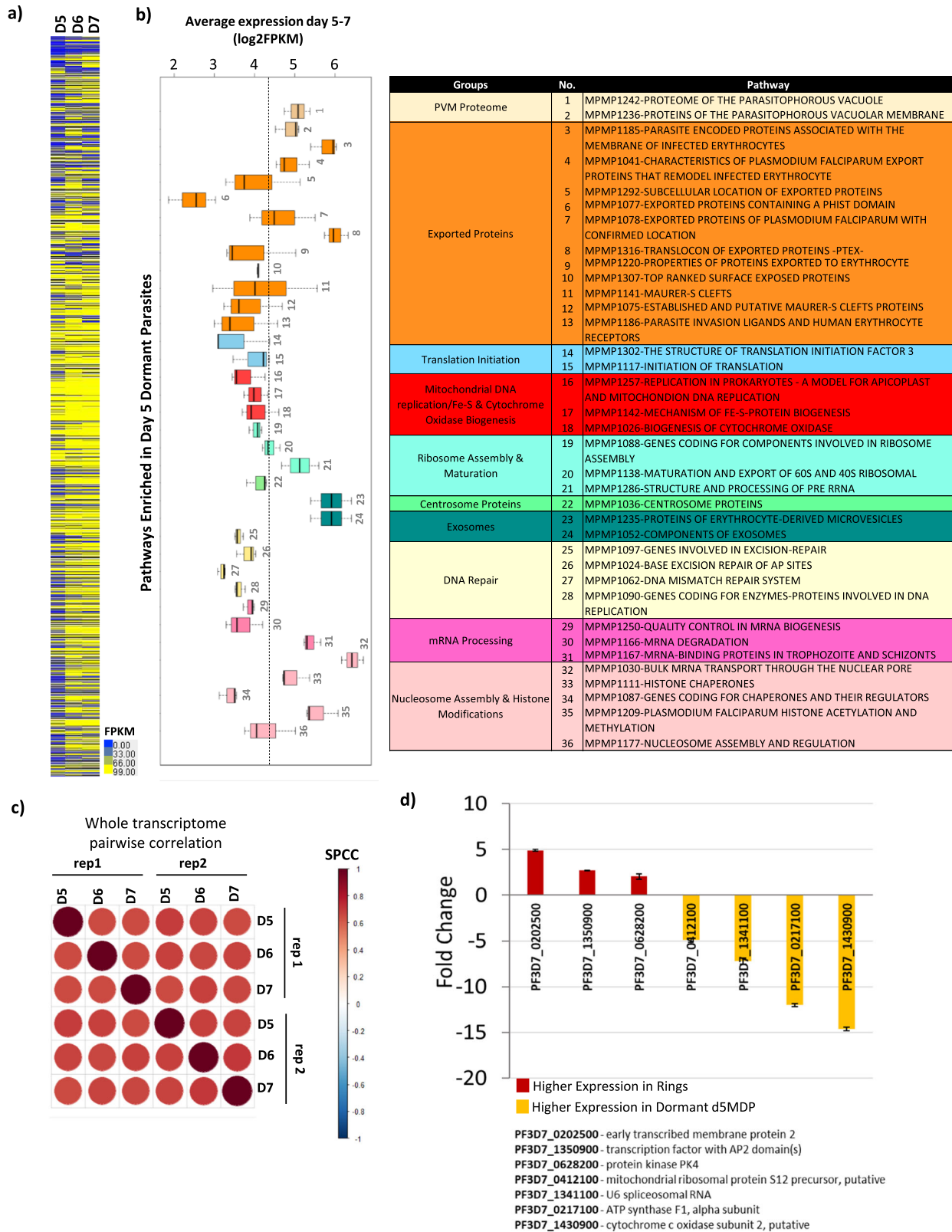### The d5MDPs represent viable cells characterized by functional mitochondria

Overall, the transcriptomic results further support our original hypothesis that the condensed forms of *P. falciparum* parasites are viable, given that these carry a highly specific transcriptional profile with a distinct set of biological functions that gets established 5 days after induction. To support this hypothesis further, we wished to investigate d5MDPs viability and, as such, their potential of reemergence to asexual growth. Our initial Giemsa stain-based evaluations suggested that essentially all condensed forms of the parasites across the experimental time course (Day1-Day5) exhibit the presence of compressed chromatin (red/purple stain) along with condensed but visible cytoplasm (blue stain) (Fig. S2A, B)[27]. To complement this, we investigated the intactness of the mitochondrial membrane potential (MMP) by the fluorescent indicator MitoTracker™. Using FACS, we observed one continuous cell population in the ring/condensed forms gate defined by the Hoechst staining (Fig. 4a). Likewise, the Mito-Tracker™ staining appeared contiguous in this population of the condensed forms from both Day 1 and Day 5 post-DHA exposure. Using the edge of the uninfected, analogous to Connelly S. V. et at (2021) as the conservative threshold[25], we observed that at least 70.6% and 74.7% of the Day 1 and Day 5 condensed forms passed this threshold, respectively. To support this, we carried out life cell imaging to compare MitoTracker™ staining between the ring stage parasites prior to DHA treatment and Day 1 and Day 5 after (Fig. S9A). Here, we conducted an unbiased quantitative analysis of the MitoTracker™ microscopy of 100 cells with DAPI nuclear signal staining for each cell sample (Supplementary Data 3). Essentially, all DAPI-stained parasites also exhibited some degree of MitoTracker signal albeit lesser intensity in Day 1 and Day 5 condensed forms compared to the ring stages (Figs. 4B and S9B). High-resolution microscopy ultimately demonstrated that the MitoTracker signal from all positive cells reflects the membrane potential within mitochondria compartments in each d5MDP juxtaposed to the nucleus (Fig. 4c). This is consistent with previous suggestions that the *P. falciparum* dormant stages contain enlarged mitochondria located near the nucleus[25].

Finally, in a recent study, Kobpornchai, P. et al.[31] showed that fluorescent staining with propidium iodide (PI) (or the lack of it) indicates an active membrane potential of the parasite cells and thus their viability[31]. In these studies, a considerable fraction of DHA-induced dormant parasites displaced PI staining as the sign of their viability, which contrasted dead parasites after paraformaldehyde-glutaraldehyde (PFA-GA) treatment that exhibited full PI positivity. Here, we employed an analogous analysis showing that essentially all DHA-induced condensed forms displace PI staining for up to 5 days, and the PFA-GA treated (dead) parasites are fully PI-positive (Fig. S10). Crucially, the initial PI-negative d5MDPs (99.75%) became PI-positive (98.92%) after PFA-GA treatment (Fig. 5a). This result is also consistent with the overall viability status of the d5MDP, showing their susceptibility to deadly treatment with PFA-GA.

d5MDPs are highly resilient to most antimalarial drugs

Considering these viability indicators, it is now feasible to investigate the level and profile of sensitivity of the d5MDPs to antimalarial drugs. To do so, we carried out a drug sensitivity assay in which d5MDPs were matured for four days and subsequently treated with a series of antimalarial drugs or inhibitory compounds at concentrations equivalent to their 1x, 10x and 100x of the 50% inhibitory concentrations (IC_{50}) determined for the IDC asexual parasite stages ($^{IDC}IC_{50}$, Fig. S11). After 24 h of exposure (completed on day 5), the drug was removed, and re-initiation of the asexual growth was monitored for up to 30 days (Fig. 5B and Supplementary Data 4). Altogether, 1x $^{IDC}IC_{50}$ treatments of the d5MDPs with most tested antimalarial drugs did not alter their recovery rate, suggesting their full resistance to these concentrations. The exceptions were amodiaquine (AMQ) and trichostatin (TSA),

a) Heatmap of Pathways Enriched in Day 5 Dormant Parasites (D5, D6, D7; FPKM scale 0.00–99.00).

b) Average expression day 5-7 (log2FPKM)

Groups	No.	Pathway
PVM Proteome	1	MPMP1242-PROTEOME OF THE PARASITOPHOROUS VACUOLE
	2	MPMP1236-PROTEINS OF THE PARASITOPHOROUS VACUOLAR MEMBRANE
Exported Proteins	3	MPMP1185-PARASITE ENCODED PROTEINS ASSOCIATED WITH THE MEMBRANE OF INFECTED ERYTHROCYTES
	4	MPMP1041-CHARACTERISTICS OF PLASMODIUM FALCIPARUM EXPORT PROTEINS THAT REMODEL INFECTED ERYTHROCYTE
	5	MPMP1292-SUBCELLULAR LOCATION OF EXPORTED PROTEINS
	6	MPMP1077-EXPORTED PROTEINS CONTAINING A PHIST DOMAIN
	7	MPMP1078-EXPORTED PROTEINS OF PLASMODIUM FALCIPARUM WITH CONFIRMED LOCATION
	8	MPMP1316-TRANSLOCON OF EXPORTED PROTEINS -PTEX-
	9	MPMP1220-PROPERTIES OF PROTEINS EXPORTED TO ERYTHROCYTE
	10	MPMP1307-TOP RANKED SURFACE EXPOSED PROTEINS
	11	MPMP1141-MAURER-S CLEFTS
	12	MPMP1075-ESTABLISHED AND PUTATIVE MAURER-S CLEFTS PROTEINS
	13	MPMP1186-PARASITE INVASION LIGANDS AND HUMAN ERYTHROCYTE RECEPTORS
Translation Initiation	14	MPMP1302-THE STRUCTURE OF TRANSLATION INITIATION FACTOR 3
	15	MPMP1117-INITIATION OF TRANSLATION
Mitochondrial DNA replication/Fe-S & Cytochrome Oxidase Biogenesis	16	MPMP1257-REPLICATION IN PROKARYOTES - A MODEL FOR APICOPLAST AND MITOCHONDION DNA REPLICATION
	17	MPMP1142-MECHANISM OF FE-S-PROTEIN BIOGENESIS
	18	MPMP1026-BIOGENESIS OF CYTOCHROME OXIDASE
Ribosome Assembly & Maturation	19	MPMP1088-GENES CODING FOR COMPONENTS INVOLVED IN RIBOSOME ASSEMBLY
	20	MPMP1138-MATURATION AND EXPORT OF 60S AND 40S RIBOSOMAL
	21	MPMP1286-STRUCTURE AND PROCESSING OF PRE RRNA
Centrosome Proteins	22	MPMP1036-CENTROSOME PROTEINS
Exosomes	23	MPMP1235-PROTEINS OF ERYTHROCYTE-DERIVED MICROVESICLES
	24	MPMP1052-COMPONENTS OF EXOSOMES
DNA Repair	25	MPMP1097-GENES INVOLVED IN EXCISION-REPAIR
	26	MPMP1024-BASE EXCISION REPAIR OF AP SITES
	27	MPMP1062-DNA MISMATCH REPAIR SYSTEM
	28	MPMP1090-GENES CODING FOR ENZYMES-PROTEINS INVOLVED IN DNA REPLICATION
mRNA Processing	29	MPMP1250-QUALITY CONTROL IN MRNA BIOGENESIS
	30	MPMP1166-MRNA DEGRADATION
	31	MPMP1167-MRNA-BINDING PROTEINS IN TROPHOZOITE AND SCHIZONTS
Nucleosome Assembly & Histone Modifications	32	MPMP1030-BULK MRNA TRANSPORT THROUGH THE NUCLEAR PORE
	33	MPMP1111-HISTONE CHAPERONES
	34	MPMP1087-GENES CODING FOR CHAPERONES AND THEIR REGULATORS
	35	MPMP1209-PLASMODIUM FALCIPARUM HISTONE ACETYLATION AND METHYLATION
	36	MPMP1177-NUCLEOSOME ASSEMBLY AND REGULATION

c) Whole transcriptome pairwise correlation (rep1, rep2; D5, D6, D7). SPCC scale −1 to 1.

d) Fold Change bar chart.

Higher Expression in Rings:
- PF3D7_0202500 - early transcribed membrane protein 2
- PF3D7_1350900 - transcription factor with AP2 domain(s)
- PF3D7_0628200 - protein kinase PK4

Higher Expression in Dormant d5MDP:
- PF3D7_0412100 - mitochondrial ribosomal protein S12 precursor, putative
- PF3D7_1341100 - U6 spliceosomal RNA
- PF3D7_0217100 - ATP synthase F1, alpha subunit
- PF3D7_1430900 - cytochrome c oxidase subunit 2, putative

which caused a delay in recovery by 5.6 days and 4.8 days on average, respectively, at 1x $^{IDC}IC_{50}$. Furthermore, d5MDPs appear resistant to even 10x and 100x $^{IDC}IC_{50}$ concentrations of atovaquone (ATQ), pyrimethamine (PMT), triclosan (TRI) (Fig. 5B, Fig. S11B). There was an intermediate effect of 10–100x $^{IDC}IC_{50}$ of DHA, MMV 1576856, (spiroindolone class) and TSA delaying the asexual growth recovery by 5–10 days. Finally, d5MDPs appear sensitive to several classes of

antimalarials, including mefloquine (MFQ), lumefantrine (LMF), amodiaquine (AMQ), and doxycycline (DOX) at 10-100X $^{IDC}IC_{50}$. In particular, 100x $^{IDC}IC_{50}$ concentrations of MFQ, LMF and AMQ that still correspond to their physiological concentrations, blocked the asexual growth recovery of the d5MDPs completely (past the 24-day observation period) or delayed by more than 20 days (Fig. 5b). The pattern of no parasite recovery was similar for 10-100x $^{IDC}IC_{50}$ LMF even when

Fig. 3 | Transcriptome and Functional Pathway Enrichment for day 5 dormant parasites (d5MDPs). a A heatmap showing expression for genes (rep 1, g_{down} and g_{up} in the same order as Fig. 2a) during the *persistence* phase (Day 6-7). Yellow color depicts higher FPKM values whereas blue depicts lower FPKM. **b** A boxplot depicting average expression (in log2FPKM, rep 1) of pathways on Day 5–7 was found to be significantly enriched during Gene Set Enrichment Analysis (GSEA) of d5MDP whole transcriptome. The boxplots are color-coded and categorized according to cellular/metabolic function similarities within the parasite (table on right). Each box represents the average expression values from first to third quartile

with the black horizontal line across each box representing the median value. The top and bottom whiskers represent the maximum and minimum values of average expression (within the 1.5 times interquartile range) respectively. **c** A bubble plot depicting whole transcriptome correlations (Spearman's Rank Correlation Coefficients, SPCC) for Day 5, 6, and 7 *persistence* phase of the parasite transcriptome (biological replicates - rep 1 and rep 2). **d** RT-PCR-based measurements of relative mRNA levels of selected genes between rings and d5MDPs. The error bars represent measurements between two biological replicas and three technical replicas from each (n = 6). Source data are provided as a Source Data file.

parasites were treated 24 h after induction of dormancy with DHA, mimicking the clinical treatment scenario (Fig. S11B). In addition to these, we tested the d5MDP toxicity of tafenoquine (TAF) which has high efficacy against the *P. vivax* liver dormant stage hypnozoites. Due to the need for in vivo metabolic conversion, the drug has a high in vitro $^{IDC}IC_{50}$ that reaches its physiological concentration (TAF ~ 500 nM, Fig. S11A). At these concentrations, tafenoquine didn't affect d5MDP reemergence. Although 10x and 100x $^{IDC}IC_{50}$ of TAF did block the growth recovery to some extent, these concentrations are clinically unrealistic, and the observed in vitro effect likely represents (some form of) general toxicity. It has been previously observed that adding gibberellic acid (GA) directly to the DHA-treated parasites promotes faster recrudescence[32]. Here, we used three different concentrations of GA (1 μM, 10 μM and 100 μM) on d5MDPs. However, in our case, GA didn't affect the recrudescence and its delay of d5MDPs (Fig. 5b).

Cellular structure characterizations of d5MDPs as a distinct *P. falciparum* life cycle developmental stage by transmission electron microscopy

Next, we studied the ultrastructure of d5MDPs by performing transmission electron microscopy post-DHA treatment on day 1, day 5 (d5MDPs) and asexual ring stages for comparison. As shown in Fig. 6a and Fig. S12, the ring stage parasites show cuplike shape with well-defined sub-cellular organelles such as the nucleus, rough endoplasmic reticulum (RER), ribosome and membranous organelles such as mitochondria (M) and Golgi apparatus (GA). In contrast, 24 h after DHA exposure (Day 1), the ring stage parasites transform into round-shaped forms with somewhat lucent areas in the cytoplasm harboring fewer ribosomes and the presence of organelles such as the GA, RER and M still identifiable (Fig. 6b and Fig. S12). d5MDPs, however, exhibit a highly irregular morphology characterized by a lack of intracellular organellar structures, the presence of large "empty" vacuole-like structures (VS) and enlarged mitochondria. There is also a reduction in the number of ribosomes in the cytoplasm, but on the other hand, massive formation of multi-membrane structures (MAS) (Fig. 6C). Several of these features have been reported previously in quinine, artesunate, and/or piperaquine-treated *P. falciparum*[33,34]; however, most of these ultrastructural studies described short-term (hours) morphological changes upon drug exposure in the trophozoite stage. It is also important to note that we also observed frequent electron-dense formations in the infected RBCs cytosol, possibly indicating packets of proteins exported by the parasite (Fig. 6d and Fig. S13). Strikingly, these packets were observed mainly in infected RBCs in day 5 samples (Figs. S13 and S14) and not uninfected RBCs, possibly indicating an active reduction in protein processing, folding and export to the host cell surface during dormancy. Overall, our results describe the long-term morphological changes in DHA-induced condensed dormant stages of *P. falciparum*.

Discussion

As opposed to the liver stage dormancy of *P. vivax*, which has been the subject of numerous studies[35], the existence of the dormant parasite forms of *P. falciparum* induced by drug exposure during the IDC is a relatively new concept. Given its potential to cause important clinical phenotypes such as recrudescence and drug resistance[17,36,37], it is

imperative to understand its biological significance fully. As shown in the earlier studies, in vitro exposures of ring-stage parasites to clinically relevant concentrations of DHA (~700 nM) can transform varying proportions of the parasite population into dormant stages[17,19,20,25,38]. The parasites remain dormant with little or no apparent signs of multiplication for at least 8 days, after which a growth recovery was reported as early as Day 10 but sometimes as late as Day 25[21,25,27,31,39]. These time differences were generally attributed to the parasite's genetic background (including drug resistance) and growth conditions at the induction time. The growth initiation originates largely from the "re-awakening" of a small portion of the dormant parasites to asexual growth, which in one study was estimated to range between 0.044% and 1.313%[19]. Nevertheless, neither of the studies could exclude a contribution of the residual asexual stage parasites that remained in the bulk cultures at small levels such as 0.9% and 8.04% for GB4 and 803 strains, respectively, in the study of Connelly S. V. et al.[25]. Finally, in approximately half of the previous reports, the total parasitemia (including the condensed forms) remained constant through the DHA-induced dormancy time course[20,22,23,31,39]. In other studies, however, the total parasitemia was reported to be near zero before the sexual growth re-emergence[19–21,25,38]. Here, we report a similar approach in which essentially all parasites persisted at the initial parasitemia for up to 8 days, after which asexual growth resumed fully on Day 10. During the *persistence* phase of the time course, a small fraction (<2%) of the parasite's population consisted of asexual forms while most (>98%) exhibited a condensed morphology, presumably reflecting dormancy, particularly at Day 5 (d5MDPs). We estimated that, in the given culturing conditions, up to 4.16% ± 3.86% of these d5MDPs have the propensity to reemerge to asexual growth while most will remain dormant and eventually die along with the host erythrocyte. Altogether, this study is reminiscent of the previous reports falling within the variation range of the culturing parameters. As mentioned above, some of these variations were attributed to the parasite's genetic background and the induction conditions. Our studies contrast all previous studies in three main aspects: (i) we used the 3D7 *P. falciparum* strain which was never used before (except D6 which is genetically related but not identical)[19]; (ii.) the DHA treatment was carried out with mid rings (6–12 HPI) while all previous studies used early rings (0-3HPI); (iii) here we adjusted the initial parasitemia to 8% which is substantially higher compared to the previous studies using 2% (Fig. 1 & S1). Hence, currently, it is unclear whether the dormancy parasites induced in these studies are identical to those induced earlier. However, it is feasible to speculate on their analogy given the overall similarities in the culture dynamics and the distribution of the morphology distribution over the experimental time course. In future studies, it will be interesting to explore further the nature of the inconsistencies in the inductions of dormancy mediated by artemisinins but possibly other conditions, including other antimalarial drugs or other external perturbations, some of which were reported previously[40,41].

The focus of this study was the mature dormant parasites which are formed after a five-day maturation process during which the initial ring-like transcriptome transforms to unique previously unobserved transcriptional profiles carrying features of quiescence and senescence simultaneously. This transcriptional transformation is striking
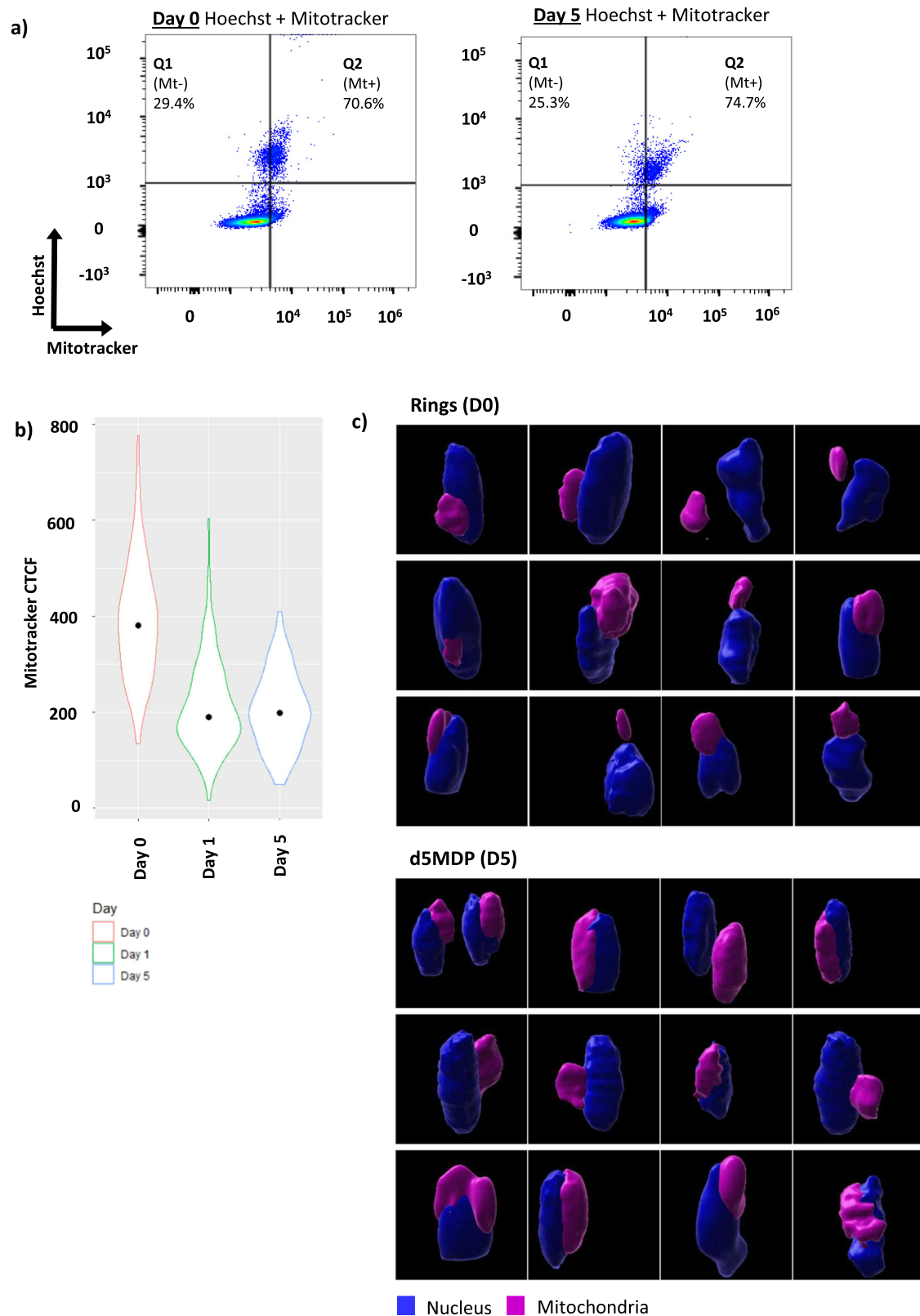
Fig. 4 | Mitotracker Staining of Day 5 post-DHA Exposure Parasites (d5MDPs) indicates viability of pyknotic parasites. a FACS plots representing Hoechst 33342 and Mitotracker Deep Red staining on Day 0 (6-12hpi rings) and Day 5 (d5MDPs). Quadrant 1 and 2 are both Hoechst-positive. Mitotracker staining positivity in Q2 was calculated as: Mt + = Q2/(Q1 + Q2)*100. This experiment was performed once. **b** Average intensity of Mitotracker Deep Red staining. The violin plot shows the average intensity of Mitotracker Deep Red stain quantified in ring stages (Day 0), Day 1 and Day 5 post-DHA treatment parasites ($n = 100$). CTCF (corrected total cell fluorescence) values calculated in ImageJ. Source data are provided as a Source Data file. **c** Staining specificity evaluation by 3D reconstruction of nucleus and mitochondrion in live parasites. Live-cell imaging pictures of untreated rings (Day 0) and d5MDPs were processed with Imaris software to generate 3D visualization of the nucleus (DAPI - blue) and mitochondrion (Mitotracker Deep Red - purple) Images are the representative selection out of ~250 cells (per condition) captured by the software.
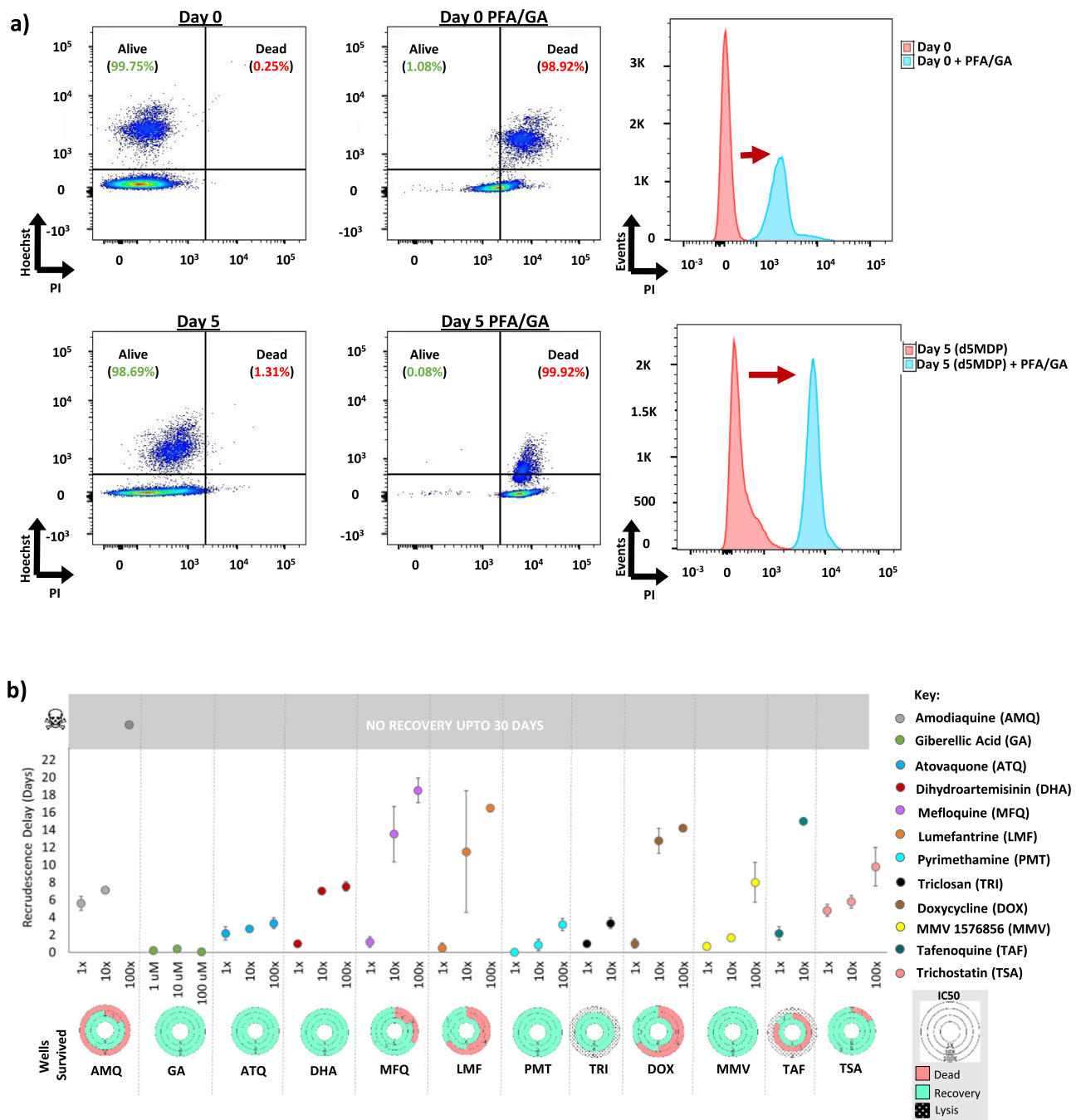
Fig. 5 | Viability evaluation using Propidium Iodine (PI) and Drug sensitivity profiling of *P. falciparum* d5MDPs. a FACS plots representing Hoechst 33342 and PI staining on Day 0 (6–12hpi rings) and Day 5 (d5MDPs) before and after paraformaldehyde + glutaraldehyde (PFA/GA) treatment. Live cells are indicated as Hoechst + /PI- in Q1 and dead cells are shown in Q2 (Hoechst + /PI +). The percentage of infected live or dead RBCs in Q1 and Q2 respectively was calculated as: Qx% = Qx/(Q1 + Q2)*100 (where Qx Q1 for live and Qx Q2 for dead infected RBCs). Histograms show the PI staining shift before and after paraformaldehyde/glutaraldehyde (PFA/GA) treatment on the corresponding day. This experiment was performed once. **b** A graph showing recrudescence delay for d5MDPs treated with various antimalarial drugs/compounds for 24 h (started on Day 4) as compared to the controls (i.e. parasites treated with the corresponding drug solvent – DMSO, methanol or water, see Fig.S11A). Three different concentrations (i.e. 1xIC50, 10xIC50, 100 x IC50) were tested per drug. Three independent biological replicates were conducted with two technical replicates per condition. Error bars indicate SEM calculated from all the cultures/wells that eventually recovered. The circular charts below show the number of cultures/wells that recovered, died (i.e. no recovery up to 30 days) or were lysed for each drug concentration tested (legend on the right). Source data are provided as a Source Data file.

given that the RNA-Seq analyses were carried out will exactly 500 cells sorted by FACS, all of which exhibited a condensed morphology from Day 1. To our knowledge, this is the first application of the "few-cell" transcriptomics, developed by our group earlier that allows transitional analyses of minute or highly specific cell samples in *Plasmodium* infections[30]. Here we characterize the transcriptome of the d5MDPs

that demonstrate their viability given its full reproducibility and specificity demonstrated in multiple biological replicas (Figs. S5–S8). Moreover, the d5MDPs carry an intact nucleus and mitochondria, which maintain their membrane potential indicated by the Mito-Tracker™ staining. This is consistent with previous observations of the dramatically enlarged mitochondria with abnormal cellular
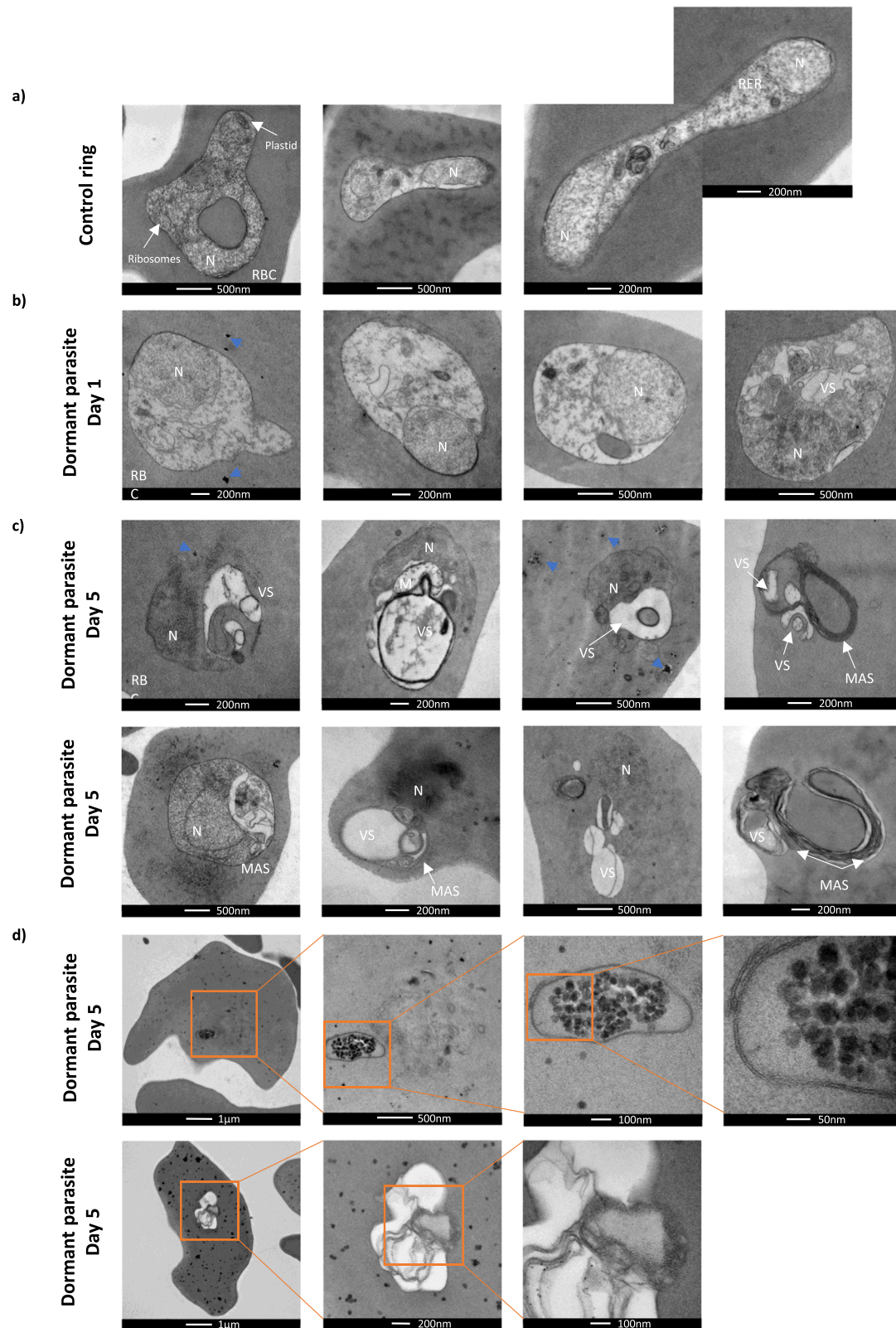
arrangement relative to the nucleus and active transcription of at least 5 mitochondria-linked genes[24,25]. This further supports the analogy between the d5MDPs and the dormant parasites characterized in the previous studies and provides further knowledge for their future analyses. Here, we show that the d5MDPs exhibit considerable resilience to a spectrum of antimalarials, including artemisinin and atovaquone. The latter is particularly surprising given the prevalent presence of mitochondria, the natural target of atovaquone, in d5MDPs. In future studies, it will be crucial to study the basic biological blueprint of the *P. falciparum* dormant forms, with a particular focus on their druggability and roles in clinical phenotypes, including artemisinin resistance (see below)[8,18,42].

The blood stage dormancy represents a physiological state of the *P. falciparum* parasite cells that are temporarily arrested in their

Fig. 6 | Transmission electron micrographs showing ultrastructure of _P. falciparum_ ring stages and post DHA treatment on Day 1 and 5. a Low-power transmission electron micrograph of ring stages with distinct organelles such as nucleus (N), ribosomes, plastid and rough endoplasmic reticulum (RER). **b** Low-power transmission electron micrograph of dormant parasites 1 day post DHA treatment, showing the transformation of parasites to round and compact forms, with the nucleus (N) being the most identifiable organelle in the parasite. Note the presence of electron dense spots in the RBC cytosol (blue arrowhead). **c** Low-power transmission electron micrograph of d5MDPs showing a completely different morphology characterized by lack of intracellular organellar structure except for

the nucleus (N) and the presence of large "vacuole-like" structures (VS) and multi-membrane structures (MAS). An increase in electron dense spots (blue arrowhead) was also observed. **d** Low-power transmission electron micrographs with increasing magnification (orange boxes) showing electron dense spots at Day 5 post DHA treatment were observed in the cytosol of 48 out of 65 infected RBCs (73%) on Day 5 (Fig. S13). Additionally, clusters of these spots surrounded by membranous structures, forming packets, were observed in d5MDP infected-RBCs. All represented TEM pictures are from two independent experiments. Approximately 100 images were generated per each day captured.

development but can ultimately recover to full growth. This is analogous to quiescence, which was reported for most (if not all) eukaryotic systems (reviewed in refs. 43, 44). Cellular quiescence ranges from reversible arrest of unicellular organisms such as yeast, during the stationary growth phase and/or sporulation[45] to metazoans in which most somatic cells are arrested in the G0 phase but could be rapidly "revived" in special situations such as wound healing[46]. Indeed, several aspects of the d5MDP transcriptome are compatible with quiescence. These include the downregulation of essentially all proliferation processes such as transcription (RNA Pol I & II-driven RNA synthesis); translation (protein synthesis, folding, trafficking and posttranslational processing); and factors involved in the host cell cytoplasm remodeling (such as the PTEX translocon and Maurer's clefts) all of which are essential for growth and development of the ring stages along the IDC[47]. This seems complemented by upregulation of some parts of the energy metabolism; biosynthesis of amino acids, lipoic and shikimate acids, and nucleotide precursors, indicating an active metabolic state of the dormant parasite stage also suggested previously[25,38]. Due to this, the blood stage dormancy is occasionally referred to as "dormant rings", implying a growth arrest in the ring stage[22]. However, this study's results somewhat contradict this vision, showing very little resemblance between the d5MDPs and the canonical ring stages. Besides the distinct transcriptome, the d5MDPs exhibit irregular cellular ultrastructure dominated by an enlarged (and active) mitochondrion, condensed nucleus, and "vacant cytoplasm" with diminished propensity of protein export, which is fundamentally different from the ring form parasites. The induction of mitochondria and suppression of glycolysis of the d5MDP also contradicts cellular quiescence, which is typically characterized by an opposite trend[48]. The ability of the _P. falciparum_ to enter cellular quiescence can be also questioned by the fact that the canonical cell cycle regulatory network based on cyclins, cyclin-dependent kinases (CDK) and cyclin inhibitors typically facilities quiescence[43] are not well conserved in the _Plasmodium_ genomes[49]. Moreover, the asexual IDC is not a standard cell cycle but rather a developmental program[47] driven by a series of transcription factors such as the ApiAP2 gene family[50].

On the other hand, the d5MDPs carry some characteristic of another arrested cellular state: senescence. Originally discovered in the 1960s[51], cellular senescence is associated with growth arrests but significant metabolic activities[52]. This is typically accompanied by broad gene expression changes facilitating the senescence state[53] (and resistance to apoptosis[54]). In higher eukaryotes, cellular senescence is triggered by shortening of the telomeres during aging[55]. Senescence can be, however, also induced by external stresses (stress-induced premature senescence)[44] such as therapeutic agents in cancer cells referred to as therapy-induced senescence (TIS)[56]. TIS is frequently triggered by DNA damage, mediated by reactive oxygen species (ROS) produced by abnormal activity of the mitochondria that in some cases is reversible[57]. The subsequent feedback loop between the DNA damage and abnormally functioning mitochondria can maintain senescence via elevated levels of ROS indefinitely[58]. Indeed, d5MDPs exhibit (abnormally) acting mitochondria (see above), which is accompanied by high transcriptional levels of genes involved not only in DNA repair machinery but also in chromatin structure such as

histone chaperones and factors of nucleosome assembly (Figs. 2B and 3B). Hence, it is tempting to speculate that the artemisinin-induced dormancy may be also maintained by an interplay between abnormally functioning mitochondria and DNA damage.

Taken together, the blood stage dormancy of _P. falciparum_ appears to combine molecular and cellular mechanisms from both cellular quiescence and senescence in a unique set of processes leading to a robust but reversible growth arrest. This process seems to involve two seemingly independent but likely tightly interlinked steps: (i.) stress (DHA)-induced conversion from the ring stage to into pyknosis and (ii.) maturation process characterized by gradual transcriptional shifts to a highly unique physiological state and subsequent re-emergence back to the ring stage and full asexual growth. The dynamics and breadth of the dormancy-related transcriptional shifts are reminiscent of other developmental processes of the _Plasmodium_ life cycle such as the asexual IDC, gametocytogenesis and/or the intrahepatocyte development in which large proportions of the genes also undergo orchestrated transactional programs[16,47,59,60]. In future studies, it will be interesting to investigate whether the dormancy-related transcriptional program is governed by a similar system of transcriptional regulators, including the ApiAP2 family of transcription factors[50]. It will also be interesting to investigate whether the blood stage dormancy shares common features with the pre-erythrocytic stages (hypnozoites) but also the dormancy of other eukaryotic species, including plants[61].

Both mitochondrial genes and DNA repair factors, two dominant functionalities of the d5MDP transcriptomes, were also implicated in artemisinin MOA and/or resistance[62-65]. Currently, there are two opposing studies associating (or not) dormancy in artemisinin resistance directly. In vitro, a _P. falciparum_ parasite line resistant to artelinic acid (W2AL80) exhibited a decreased propensity to fall dormant as they were able to better tolerate the drug exposure and continued to grow despite the drug treatment[38]. On the other hand, the presence of the artemisinin resistance-linked PfK13 mutations does not seem to modulate dormancy after artemisinin induction and/or sorbitol treatment[39]. Hence, the role of the dormant blood stage _P. falciparum_ parasite in the disease progression and treatment outcome is still a matter of debate[36,42]. In a recent opinion article, Wellems, T. et al.[36] argued that the persister parasites are unlikely to be associated with the increased parasite clearance halftimes ($^{1/2}$PC), the current phenotypic feature of artemisinin resistance[36]. Indeed, there appears to be no association between $^{1/2}$PC and recrudescence and longer $^{1/2}$PC do not cause delayed resolutions of malaria infections[66]. On the other hand, there is mounting evidence that dormant parasites occur in vivo, in humans[27], and in rodent models[26]. In the latter study, the growth recovery time was directly correlated to the dose of dormant parasites transferred to the rodent host, suggesting their significance in recrudescence. Hence, even though dormancy might not be the main direct factor in artemisinin resistance mediated by PfK13 mutations, it may play significant a role in the rapidly spreading ACT failures in the GMS[7].

The resilience of the d5MDPs to a broad spectrum of antimalaria drugs might indeed be a key factor of this phenomenon, allowing residual fractions of dormant parasites to survive an ACT course. The d5MDPs appear to be fully resistant to all or most tested antimalaria

drugs when applied at ^{IDC}IC50 and 10x^{IDC}IC50 for asexual growth, respectively. Only 100x^{IDC}IC50 of AMQ, LMF, MF and DOX were able to either kill or significantly impede the d5MDP growth re-emergence. Indeed, three quinolines, MFQ, AMQ of LMF are the most frequently used as the long-lasting partner drugs of the current ACT and the tested 100x^{IDC}IC50 concentrations are clinically relevant that could affect the dormant parasites (Fig. S11)[10,67,68]. The mode of action (MOA) of the three quinolines is believed to mainly involve inhibition of heme polymerization and thus production of ferriprotorphyrin IX that is highly toxic to asexual forms of *Plasmodium* parasites[69]. However, hemoglobin digestion is unlikely to take place in the dormant parasites suggesting that the inhibiting quinoline effects are mediated by other components of their presumed pluripotent MOAs[70,71]. In particular, mefloquine is also known to target components of the *Plasmodium* cytoplasm such as the ribosome Pf80S[72], PfPnP[73], an AcetylCoA-binding protein[74] and possibly other mechanisms leading to inductions of ROS and subsequent apoptosis[75]. Mefloquine is also potent against other parasites that do not rely on blood ingestion, such as tapeworms (*Echinococcus multilocularis*)[76] and nematodes (*Schistosoma mansoni*)[77], possibly by targeting crucial metalloproteins. Similarly, amodiaquine and lumefantrine were suggested to some degree also act via targets outside of the digestive vacuole possibly by interfering with DNA and protein synthesis[71]. Hence inhibition of the *P. falciparum* dormant parasites by the three quinolines is likely to be also mediated by at least some of these cytoplasmic effects. Moreover, the main target of doxycycline antimalaria activity is apicoplast protein synthesis, causing delayed[78] or immediate parasite death depending on the drug dose[79]. The transcriptome of the d5MDP indicates upregulations of genes associated with apicoplast which is consistent with the doxycycline inhibitory effect. The absolute inactivity of atovaquone against the dormant parasite is counterintuitive, given that its main target is the mitochondria-located Bc1 complex of the *P. falciparum* oxidative respiratory chain[80]. This indicates that even though the mitochondria are the predominant features of the dormant parasites, inhibition of its respiratory chain does affect their viability. As such atovaquone appears unsuitable as a candidate ACT partner drug. From that end, we wish to propose that future ACT combinations take into consideration partner drugs with higher capacity to eliminate the d5MDPs to prevent recrudescence along with increasing frequencies of ACT failures. One such strategy includes the design of triple artemisinin combination therapies (TACT) that are currently being evaluated for their ability to prevent the rise of resistant parasites[81].

Methods

Parasite culture and dormancy induction

3D7, DD2, W2 strains (MR4) and T996 (laboratory strain) of *Plasmodium falciparum* were cultured in RPMI 1640 medium (Gibco) containing purified human packed RBCs, supplemented 1with 0.25% Albumax II (Gibco), 0.1 mM hypoxanthine (Sigma), Sodium bicarbonate (Sigma) (2 g/L), and gentamicin (Gibco) (50 µg/L). Cultures were maintained on the shaker at 37 °C with 5% CO_2, 3% O_2, and 92% N_2 in 2% hematocrit. The culture medium was replenished regularly at least every 24 h, fresh RBCs were added once a week. Blood smears fixed with 100% Methanol (Fisher Chemical) and stained with 10% Giemsa (Sigma) for 3 min were used for microscopy examination. For the distinct differentiation of nucleus and cytoplasm of dead vs. dormant condensed forms, Giemsa was filtered before the staining using the 0.2 µM syringe filter (Pall Life Science), diluted into 5% concentration and smears were stained for 20 min instead. For parasitemia calculation, 500 RBCs were counted in at least five view fields and if parasitemia was below 1%, ~10,000 RBCs were counted instead.

Parasite culture containing ring stages was synchronized in two consecutive cycles before the start of the experiments via 5% sorbitol (Sigma) to achieve a maximum age difference of ~6 h.

Dormancy was induced by adding 700 nM Dihydroartemisinin (DHA) to the 6–12 HPI parasite rings for 6 h. After this incubation period, the RBCs were washed 3x with warm RPMI media to remove the DHA thoroughly. Mature parasites unaffected by the treatment were removed by passing the culture through a magnetic column (MACS) for three consecutive days after the drug treatment, as described elsewhere[19].

Flow cytometry, sorting strategy, and RNA sequencing

Staining of the samples for the flow cytometry was performed as described elsewhere[28]. Briefly, 1 µL (for well-plate) or 10 µL (for tube) of *P. falciparum*-infected RBCs were added to the 50 µL (well-plate) or 200 µL of PBS respectively, containing 5 µg/mL Dihydroethidium (DHE) (Sigma) and 8 µM Hoechst 33342 (Thermo Scientific). DHE was used as a redox indicator and Hoechst for DNA visualization. For the viability assay, 1 µM Mitotracker Deep Red (Thermo Scientific; abs/em ~644/665 nm) was used instead of DHE as an indicator of ΔΨm. In a separate experiment, 10 µg/mL Propidium iodide (PI) (Thermo Scientific; abs/em ~493/636 nm) was used as an indicator of apoptosis. Samples were incubated for 30 min at 37 °C. An additional 200 µL (well-plates) or 3 mL (tubes) of PBS were added after the incubation.

Fortessa X20 (BD) was used to acquire all flow cytometry data using the UV laser (355 nm excitation) for Hoechst 33342 detection, blue laser (488 nm excitation) for the DHE and PI, and the red laser (633 nm) for the Mitotracker Deep Red. 50,000 events were recorded for each sample and FlowJo (Tree Star) was used for FACS data processing (specifically, for excluding the debris and doublets and for gating of the parasites, as shown in Malleret et al.[28]). Uninfected RBCs were stained as a negative control.

500 infected RBCs were sorted into 3 µL of Lysis buffer (final concentration of RNAseOut 2 U/µL and 1 mg/mL BSA, Molecular Biology Grade (NEB), diluted into sterile PBS) by FACSAria II (BD) into 0.2 mL PCR strip tubes. Sorted samples were spun briefly and processed afterward for RNA extraction or stored at −80 °C. To confirm the correct sorting and gating strategy, 3000–5000 cells were collected from each gate into 3 µL of RPMI media. 1 µL of packed blood was diluted into 9 µL of RPMI media in a separate tube to prepare ~1 million RBCs/1 µL. Then, 1 µL of diluted blood was added to the tube with the sorted cells to achieve 0.3–0.5 % parasitemia. The tube was briefly spun afterwards, and a short blood smear was made and stained by Giemsa to evaluate the stage of the sorted parasites in the corresponding sample (Fig. 1B).

For RNA sequencing, 500 sorted cell lysate was subjected to SMART-Seq2 protocol as stated elsewhere[30] with minor modifications. Briefly, RNA priming was performed by incubating the cell lysate with 1 mM dNTP and 1 µM Oligo-dT30VN at 72 °C for 3 min in a preheated thermal cycler. Samples were put back on ice immediately after incubation. Following this, a reverse transcription mix was prepared containing 120U of SuperScript™ II Reverse Transcriptase (Invitrogen™), 12U RNaseOUT™ Recombinant Ribonuclease Inhibitor (Invitrogen™), DTT (5 mM), betaine (1 M), MgCl2 (6 mM), LNA-TSO (1 µM) and nuclease-free water and added to the primed lysate. Samples were then incubated according to the SMART-seq2 reverse transcription and cDNA amplification protocol[30], with certain adaptations for the dormant stages of *Plasmodium* (Supplementary protocol). Sequencing libraries were generated by Illumina Nextera XT kit and DNA/RNA UD Indexes (Illumina) following the manufacturer's protocol. Successful tagmentation and library size were verified by Bioanalyzer High Sensitivity DNA chips (Agilent). Libraries were pooled and sequenced on the Illumina NovaSeq 6000 platform, generating ~8 Gb data output per sample. Quality metrics for RNA sequencing results are shown in Fig. S15.

Quantitative RT-PCR

100 μL of high-parasitemia culture (~30%) was used for the RNA extraction. 200 μL of DNA/RNA Shield (Zymo) and 300 μL of TRIzol (Thermo Fisher Scientific) were added to the blood and the sample was processed as stated elsewhere (Steps 2–7 and 10–36 in Supplementary protocol Kucharski et al.[30]). 50 ng of total RNA was used for reverse transcription. qRT-PCR was performed using the SYBR™ Select Master Mix (Applied Biosystems™). Forward and reverse primers were designed by the Primer3 program and ordered in desalted condition from Integrated DNA Technology.

In vitro Drug susceptibility assays

Three biological replicates of 6–12 HPI *Plasmodium* culture at 1% parasitemia, and 2% haematocrit were exposed for 48 h to 11 different concentrations of selected drugs (Fig. S11) in two-fold serial dilution manner in 96-well plate format. Each biological replicate was performed in two technical replicates. 0.1% DMSO (Sigma) was used as a negative control. After 48 h of drug treatment, cultures were washed 3x with fresh warm RPMI media. The growth of the parasites was determined after 72 h by Flow Cytometry with Hoechst 33342 and DHE staining as stated above. For all the compounds, the IC_{50} values of each biological replicate were determined by nonlinear regression analysis in GraphPad Prism 8. These IC_{50} values of all biological replicates for a specific drug treatment were then averaged and IC_{50} range interval ± SD was defined (Fig. S11).

Double drug recovery assay

6-12 HPI rings were treated by 700 nM DHA for 6 h on Day 0. Removal of mature IDC stages by MACS was conducted on Days 1–3. The culture was then treated on Day 4 with a partner drug for 24 h (Fig. S11) with three different concentrations, $1xIC_{50}$, $10xIC_{50}$, and $100xIC_{50}$. Drugs were washed off three times by fresh warm RPMI on Day 5, followed by the addition of fresh blood. Fresh blood was subsequently added every 7 days to prevent blood lysis. 1 μL of culture was stained with Hoechst 33342 and DHE for flow cytometry on Days 8–12 and every three following days until Day 30 (50,000 events recorded). The recovery day of each specific well in the well plate was determined as a higher event value of trophozoites and schizonts in culture (total amount of events in Q2) than a background value in uninfected blood controls determined by FACS (0.014–0.032). If the positive recovery reading was followed by a negative one, the culture wasn't considered as recovered (false positive). Recovery delay was calculated as a subtraction of recovery day and negative control recovery day (culture treated with 700 nM DHA on Day 0 for 6 h and with drug solvents added for 24 h on Day 4 instead of a partner drug with a corresponding concentration → DMSO, H2O, MetOH). Cultures without any trophozoites or schizonts on Day 30 were considered as not recovered.

Live cell imaging

10 μL of infected RBCs were washed with PBS, followed by staining with 100 nM Mitotracker™ Deep Red (Thermo Scientific; abs/em ~644/665 nm) and 8 μM Hoechst 33342 (Thermo Scientific; abs/em 350/460–490 nm) for exactly 30 min. Cells were washed 3x with PBS afterward, diluted with PBS into ~10% hematocrit and pipetted on the glass slide, covered with a cover slip, and fixed with a nail polish. Images were captured with a Zeiss LSM980 confocal microscope equipped with an Airyscan 2 detector using Plan-Apochromat 100x/1.46 oil objective. Images were processed using Zen 3.4 software (Carl Zeiss) for 2D projection. Imaris v.9.2 software was used for the generation of 3D images, and contrast and brightness settings were adjusted uniformly across all the processed images. Nucleus and mitochondrion volumes were visualized to determine the Mitotracker™ Deep Red staining specificity. 100 cells from Day 0, Day 1 and Day 5 were selected based on the DAPI staining threshold of 1% and Analyze particles (Size = 100-infinity) function in ImageJ. CTCF (corrected total cell fluorescence) values indicating fluorescence intensity for DAPI and Mitotracker Deep Red were calculated as follows: CTCF = (area of selected cell*mean intensity)-(area of selected cell*mean fluorescence of background). 5 different areas without fluorescence signal were selected to calculate mean fluorescence of the background on each processed figure.

Recrudescence assay

d5MDPs were seeded into the 96-well plates (2% hematocrit) in 4 different population sizes (250,000/well, 100,000/well, 50,000/well, and 10,000/well) on Day 5 after DHA treatment. Wells were then sampled every 2 days and data were collected from FACS to determine the recrudescence. Fresh blood was added to the wells every 7 days to prevent lysis. Recrudesce was observed based on the following criteria: parasitemia level >0.02%, Q2 % (proportion of trophozoites and schizonts in the culture >20%), and subsequently increasing total parasitemia (Fig. S3).

Data analysis and clustering

Raw reads obtained from the Illumina sequencer were trimmed using TrimGalore to create a high-quality read set without the contamination of primers, adapters, and low-quality bases at the 3′ ends. These reads were then aligned to the *Plasmodium falciparum* 3D7 reference genome (v3) obtained from the PlasmoDB database using HiSAT2. Properly oriented paired reads mapped to the unique location of the genome were considered for counting. BEDTools software was used to calculate gene-specific read counts which were further converted into normalized counts - Fragments Per Kilobase per Million mapped reads (FPKMs). These FPKM values were used for subsequent transcriptomic analysis. Considering the periodic nature of the gene expression profile of *Plasmodium falciparum* during intra-erythrocytic developmental stages, the expression profile of dormant stages was modeled using the Fast Fourier Transform method by fft() function in R (Supplementary Software 1). Fourier analysis on each expression profile of the transcripts was performed as described previously[43]. In brief, this method was applied for each gene's expression profile with no missing data point to obtain a high-quality dormant stage transcriptome. Fast Fourier transformed gene-expression profile calculated the relative timing of the maximum expression called phase ranged from −π to +π. Expression profiles of the genes were sorted according to these phases determined and visualized through the TreeView software. The script used for the Fourier transformation of gene expression is provided as supplementary information.

Electron microscopy

15 μL of packed RBCs from *P. falciparum* cultures (post DHA treatment on day 1, day 5, and control ring stages) were fixed overnight in 2.5% glutaraldehyde (Ted Pella, Inc.) in PBS, pH 7.3, washed in buffer, post-fixed for 1 h in 1% osmium tetroxide with 1.5% Potassium Ferrocyanide in PBS, block stained for 1 h in aqueous 1% uranyl acetate, then dehydrated in an ethanol series, absolute acetone and embedded in Araldite 502 resin (Ted Pella, Inc). Ultra-sections were cut at 90 nm on a Leica EM UC6 Ultramicrotome, collected on 200 mesh copper grids covered with a Formvar carbon support film (Electron Microscopy Sciences), and stained for 8 min in lead citrate stain. Photographs were taken with Transmission Electron Microscopy (Tecnai Spirit G2, FEI, USA) at 100 kV with a bottom mounted digital camera FEI Eagle (4k x 4k pixels).

Reporting summary

Further information on research design is available in the Nature Portfolio Reporting Summary linked to this article.

Data availability

The RNA sequencing data generated during this study have been deposited on the GEO database under the GEO accession ID for the GSE225340. All other source data are provided with this paper.

Code availability

The code generated during this study has not been deposited in a public repository because most tools used for analysis are publicly available or previously published. The Fast Fourier Transform code is provided with the Source Data file.

References

1. World Health Organization. World malaria report (2021).
2. Ashley, E. A. et al. Spread of artemisinin resistance in Plasmodium falciparum malaria. *N. Engl. J. Med.* **371**, 411–423 (2014).
3. Dondorp, A. M. et al. Artemisinin resistance in *Plasmodium falciparum* malaria. *N. Engl. J. Med.* **361**, 455–467 (2009).
4. Uwimana, A. et al. Association of *Plasmodium falciparum* kelch13 R561H genotypes with delayed parasite clearance in Rwanda: an open-label, single-arm, multicentre, therapeutic efficacy study. *Lancet Infect. Dis.* **21**, 1120–1128 (2021).
5. Stokes, B. H. et al. *Plasmodium falciparum* K13 mutations in Africa and Asia impact artemisinin resistance and parasite fitness. *Elife*. **10**, https://doi.org/10.7554/eLife.66277 (2021).
6. Uwimana, A. et al. Emergence and clonal expansion of in vitro artemisinin-resistant *Plasmodium falciparum* kelch13 R561H mutant parasites in Rwanda. *Nat. Med.* **26**, 1602–1608 (2020).
7. Dhorda, M., Amaratunga, C. & Dondorp, A. M. Artemisinin and multidrug-resistant *Plasmodium falciparum* - a threat for malaria control and elimination. *Curr. Opin. Infect. Dis.* **34**, 432–439 (2021).
8. Fairhurst, R. M. et al. Artemisinin-resistant malaria: research challenges, opportunities, and public health implications. *Am. J. Trop. Med Hyg.* **87**, 231–241 (2012).
9. Rasmussen, C., Alonso, P. & Ringwald, P. Current and emerging strategies to combat antimalarial resistance. *Expert Rev. Anti Infect. Ther.* **20**, 353–372 (2022).
10. Nosten, F. & White, N. J. Artemisinin-based combination treatment of falciparum malaria. *Am. J. Trop. Med Hyg.* **77**, 181–192 (2007).
11. Yeung, S., Pongtavornpinyo, W., Hastings, I. M., Mills, A. J. & White, N. J. Antimalarial drug resistance, artemisinin-based combination therapy, and the contribution of modeling to elucidating policy choices. *Am. J. Trop. Med Hyg.* **71**, 179–186 (2004).
12. White, N. J. Antimalarial drug resistance. *J. Clin. Invest* **113**, 1084–1092 (2004).
13. Meshnick, S. R. Artemisinin: mechanisms of action, resistance and toxicity. *Int J. Parasitol.* **32**, 1655–1660 (2002).
14. Ittarat, W. et al. Recrudescence in artesunate-treated patients with falciparum malaria is dependent on parasite burden not on parasite factors. *Am. J. Trop. Med Hyg.* **68**, 147–152 (2003).
15. Zou, J., Peng, B., Qu, J. & Zheng, J. Are Bacterial Persisters Dormant Cells Only? *Front Microbiol.* **12**, 708580 (2021).
16. Lee, W. C. et al. *Plasmodium falciparum* rosetting protects schizonts against artemisinin. *EBioMedicine* **73**, 103680 (2021).
17. Codd, A., Teuscher, F., Kyle, D. E., Cheng, Q. & Gatton, M. L. Artemisinin-induced parasite dormancy: a plausible mechanism for treatment failure. *Malar. J.* **10**, 56 (2011).
18. Kyle, D. E., Webster, H.K. In *XIVth International Congress for Tropical Medicine and Malaria, 1996*.
19. Teuscher, F. et al. Artemisinin-induced dormancy in *Plasmodium falciparum*: duration, recovery rates, and implications in treatment failure. *J. Infect. Dis.* **202**, 1362–1368 (2010).
20. Tucker, M. S., Mutka, T., Sparks, K., Patel, J. & Kyle, D. E. Phenotypic and genotypic analysis of in vitro-selected artemisinin-resistant progeny of *Plasmodium falciparum*. *Antimicrob. Agents Chemother.* **56**, 302–314 (2012).
21. Hott, A. et al. Artemisinin-resistant *Plasmodium falciparum* parasites exhibit altered patterns of development in infected erythrocytes. *Antimicrob. Agents Chemother.* **59**, 3156–3167 (2015).
22. Chen, N. et al. Fatty acid synthesis and pyruvate metabolism pathways remain active in dihydroartemisinin-induced dormant ring stages of *Plasmodium falciparum*. *Antimicrob. Agents Chemother.* **58**, 4773–4781 (2014).
23. Gray, K. A. et al. Correlation between Cyclin Dependent Kinases and Artemisinin-Induced Dormancy in *Plasmodium falciparum* In Vitro. *PLoS One* **11**, e0157906 (2016).
24. Peatey, C. L. et al. Mitochondrial Membrane Potential in a Small Subset of Artemisinin-Induced Dormant *Plasmodium falciparum* Parasites In Vitro. *J. Infect. Dis.* **212**, 426–434 (2015).
25. Connelly et al. Restructured Mitochondrial-Nuclear Interaction in *Plasmodium falciparum* Dormancy and Persister Survival after Artemisinin Exposure. *mBio* **12**, e0075321 (2021).
26. LaCrue, A. N., Scheel, M., Kennedy, K., Kumar, N. & Kyle, D. E. Effects of artesunate on parasite recrudescence and dormancy in the rodent malaria model *Plasmodium vinckei*. *PLoS One* **6**, e26689 (2011).
27. Peatey, C. et al. Dormant Plasmodium falciparum Parasites in Human Infections Following Artesunate Therapy. *J. Infect. Dis.* **223**, 1631–1638 (2021).
28. Malleret, B. et al. A rapid and robust tri-color flow cytometry assay for monitoring malaria parasite development. *Sci. Rep.* **1**, 118 (2011).
29. Tripathi, J., Zhu, L., Nayak, S., Stoklasa, M. & Bozdech, Z. Stochastic expression of invasion genes in *Plasmodium falciparum* schizonts. *Nat. Commun.* **13**, 3004 (2022).
30. Kucharski, M. et al. A comprehensive RNA handling and transcriptomics guide for high-throughput processing of *Plasmodium* blood-stage samples. *Malar. J.* **19**, 363 (2020).
31. Kobpornchai, P., Imwong, M. & Kulkeaw, K. Trio fluorophore-based phenotypic assay for the detection of artemisinin-induced growth-arrested *Plasmodium falciparum* in human erythrocytes. *Sci. Rep.* **14**, 1802 (2024).
32. Duvalsaint, M. & Kyle, D. E. Phytohormones, Isoprenoids, and Role of the Apicoplast in Recovery from Dihydroartemisinin-Induced Dormancy of *Plasmodium falciparum*. *Antimicrob Agents Chemother* **62**, https://doi.org/10.1128/AAC.01771-17 (2018).
33. Sachanonta, N. et al. Ultrastructural and real-time microscopic changes in *P. falciparum*-infected red blood cells following treatment with antimalarial drugs. *Ultrastruct. Pathol.* **35**, 214–225 (2011).
34. del Pilar Crespo, M. et al. Artemisinin and a series of novel endoperoxide antimalarials exert early effects on digestive vacuole morphology. *Antimicrob. Agents Chemother.* **52**, 98–109 (2008).
35. Schafer, C., Zanghi, G., Vaughan, A. M. & Kappe, S. H. I. *Plasmodium vivax* latent liver stage infection and relapse: biological insights and new experimental Tools. *Annu Rev. Microbiol* **75**, 87–106 (2021).
36. Wellems, T. E., Sa, J. M., Su, X. Z., Connelly, S. V. & Ellis, A. C. Artemisinin resistance': something new or old? something of a misnomer? *Trends Parasitol.* **36**, 735–744 (2020).
37. Witkowski, B. et al. Increased tolerance to artemisinin in *Plasmodium falciparum* is mediated by a quiescence mechanism. *Antimicrob. Agents Chemother.* **54**, 1872–1877 (2010).
38. Teuscher, F., Chen, N., Kyle, D. E., Gatton, M. L. & Cheng, Q. Phenotypic changes in artemisinin-resistant *Plasmodium falciparum* lines in vitro: evidence for decreased sensitivity to dormancy and growth inhibition. *Antimicrob. Agents Chemother.* **56**, 428–431 (2012).
39. Breglio, K. F. et al. Kelch Mutations in *Plasmodium falciparum* Protein K13 Do Not Modulate Dormancy after Artemisinin Exposure and Sorbitol Selection In Vitro. *Antimicrob Agents Chemother.* **62**, https://doi.org/10.1128/AAC.02256-17 (2018).
40. Nakazawa, S., Kanbara, H. & Aikawa, M. *Plasmodium falciparum*: recrudescence of parasites in culture. *Exp. Parasitol.* **81**, 556–563 (1995).
41. Nakazawa, S., Maoka, T., Uemura, H., Ito, Y. & Kanbara, H. Malaria parasites giving rise to recrudescence in vitro. *Antimicrob. Agents Chemother.* **46**, 958–965 (2002).

42. Cheng, Q., Kyle, D. E. & Gatton, M. L. Artemisinin resistance in *Plasmodium falciparum*: a process linked to dormancy? *Int J. Parasitol. Drugs Drug Resist* **2**, 249–255 (2012).

43. Marescal, O. & Cheeseman, I. M. Cellular Mechanisms and Regulation of Quiescence. *Dev. Cell* **55**, 259–271 (2020).

44. Truskowski, K., Amend, S. R. & Pienta, K. J. Dormant cancer cells: programmed quiescence, senescence, or both? *Cancer Metastasis Rev.* **42**, 37–47 (2023).

45. Opalek, M. et al. A Systematic Review on Quiescent State Research Approaches in S. cerevisiae. *Cells* **12**, https://doi.org/10.3390/cells12121608 (2023).

46. de Morree, A. et al. Staufen1 inhibits MyoD translation to actively maintain muscle stem cell quiescence. *Proc. Natl. Acad. Sci. USA* **114**, E8996–E9005 (2017).

47. Bozdech, Z. et al. The transcriptome of the intraerythrocytic developmental cycle of *Plasmodium falciparum*. *PLoS Biol.* **1**, E5 (2003).

48. Ho, T. T. et al. Autophagy maintains the metabolism and function of young and old stem cells. *Nature* **543**, 205–210 (2017).

49. Adderley, J. & Doerig, C. Comparative analysis of the kinomes of *Plasmodium falciparum, Plasmodium vivax* and their host Homo sapiens. *BMC Genomics* **23**, 237 (2022).

50. Painter, H. J., Campbell, T. L. & Llinas, M. The Apicomplexan AP2 family: integral factors regulating *Plasmodium* development. *Mol. Biochem Parasitol.* **176**, 1–7 (2011).

51. Hayflick, L. & Moorhead, P. S. The serial cultivation of human diploid cell strains. *Exp. Cell Res.* **25**, 585–621 (1961).

52. Serrano, M., Lin, A. W., McCurrach, M. E., Beach, D. & Lowe, S. W. Oncogenic ras provokes premature cell senescence associated with accumulation of p53 and p16INK4a. *Cell* **88**, 593–602 (1997).

53. Zhang, H., Pan, K. H. & Cohen, S. N. Senescence-specific gene expression fingerprints reveal cell-type-dependent physical clustering of up-regulated chromosomal loci. *Proc. Natl. Acad. Sci. USA* **100**, 3251–3256 (2003).

54. Hampel, B., Malisan, F., Niederegger, H., Testi, R. & Jansen-Durr, P. Differential regulation of apoptotic cell death in senescent human cells. *Exp. Gerontol.* **39**, 1713–1721 (2004).

55. Campisi, J. & d'Adda di Fagagna, F. Cellular senescence: when bad things happen to good cells. *Nat. Rev. Mol. Cell Biol.* **8**, 729–740 (2007).

56. Schmitt, C. A. et al. A senescence program controlled by p53 and p16INK4a contributes to the outcome of cancer therapy. *Cell* **109**, 335–346 (2002).

57. Martini, H. & Passos, J. F. Cellular senescence: all roads lead to mitochondria. *FEBS J.* https://doi.org/10.1111/febs.16361 (2022).

58. Passos, J. F. et al. Feedback between p21 and reactive oxygen production is necessary for cell senescence. *Mol. Syst. Biol.* **6**, 347 (2010).

59. Cruz Camacho, A. et al. High-throughput analysis of the transcriptional patterns of sexual genes in malaria. *Parasit. Vectors* **16**, 14 (2023).

60. Zanghi, G. et al. Global gene expression of human malaria parasite liver stages throughout intrahepatocytic development. *bioRxiv*. https://doi.org/10.1101/2023.01.05.522945 (2023).

61. Merrick, C. J. Hypnozoites in Plasmodium: Do Parasites Parallel Plants? *Trends Parasitol.* **37**, 273–282 (2021).

62. Goyal, M. et al. An SR protein is essential for activating DNA repair in malaria parasites. *J. Cell Sci.* **134**, https://doi.org/10.1242/jcs.258572 (2021).

63. Gupta, D. K., Patra, A. T., Zhu, L., Gupta, A. P. & Bozdech, Z. DNA damage regulation and its role in drug-related phenotypes in the malaria parasites. *Sci. Rep.* **6**, 23603 (2016).

64. Mok, S. et al. Artemisinin-resistant K13 mutations rewire *Plasmodium falciparum*'s intra-erythrocytic metabolic program to enhance survival. *Nat. Commun.* **12**, 530 (2021).

65. Xiong, A. et al. K13-Mediated Reduced Susceptibility to Artemisinin in *Plasmodium falciparum* Is Overlaid on a Trait of Enhanced DNA Damage Repair. *Cell Rep.* **32**, 107996 (2020).

66. Bethell, D. et al. Artesunate dose escalation for the treatment of uncomplicated malaria in a region of reported artemisinin resistance: a randomized clinical trial. *PLoS One* **6**, e19283 (2011).

67. Piedade, R. & Gil, J. P. The pharmacogenetics of antimalaria artemisinin combination therapy. *Expert Opin. Drug Metab. Toxicol.* **7**, 1185–1200 (2011).

68. Sinclair, D., Zani, B., Donegan, S., Olliaro, P. & Garner, P. Artemisinin-based combination therapy for treating uncomplicated malaria. *Cochrane Database Syst. Rev.* **2009**, CD007483 (2009).

69. Zhang, J., Krugliak, M. & Ginsburg, H. The fate of ferriprotorphyrin IX in malaria infected erythrocytes in conjunction with the mode of action of antimalarial drugs. *Mol. Biochem Parasitol.* **99**, 129–141 (1999).

70. Foley, M. & Tilley, L. Quinoline antimalarials: mechanisms of action and resistance and prospects for new agents. *Pharm. Ther.* **79**, 55–87 (1998).

71. Tisnerat, C., Dassonville-Klimpt, A., Gosselet, F. & Sonnet, P. Antimalarial Drug Discovery: From Quinine to the Most Recent Promising Clinical Drug Candidates. *Curr. Med Chem.* **29**, 3326–3365 (2022).

72. Wong, W. et al. Mefloquine targets the *Plasmodium falciparum* 80S ribosome to inhibit protein synthesis. *Nat. Microbiol* **2**, 17031 (2017).

73. Dziekan, J. M. et al. Identifying purine nucleoside phosphorylase as the target of quinine using cellular thermal shift assay. *Sci. Transl. Med.* **11**, https://doi.org/10.1126/scitranslmed.aau3174 (2019).

74. Kumar, A., Ghosh, D. K., Ali, J. & Ranjan, A. Characterization of Lipid Binding Properties of *Plasmodium falciparum* Acyl-Coenzyme A Binding Proteins and Their Competitive Inhibition by Mefloquine. *ACS Chem. Biol.* **14**, 901–915 (2019).

75. Gunjan, S. et al. Mefloquine induces ROS mediated programmed cell death in malaria parasite: *Plasmodium*. *Apoptosis* **21**, 955–964 (2016).

76. Rufener, R. et al. Activity of mefloquine and mefloquine derivatives against *Echinococcus multilocularis*. *Int J. Parasitol. Drugs Drug Resist* **8**, 331–340 (2018).

77. Manneck, T., Keiser, J. & Muller, J. Mefloquine interferes with glycolysis in schistosomula of *Schistosoma mansoni* via inhibition of enolase. *Parasitology* **139**, 497–505 (2012).

78. Kennedy, K. et al. Delayed death in the malaria parasite *Plasmodium falciparum* is caused by disruption of prenylation-dependent intracellular trafficking. *PLoS Biol.* **17**, e3000376 (2019).

79. Okada, M., Guo, P., Nalder, S. A. & Sigala, P. A. Doxycycline has distinct apicoplast-specific mechanisms of antimalarial activity. *Elife*. **9**, https://doi.org/10.7554/eLife.60246 (2020).

80. Birth, D., Kao, W. C. & Hunte, C. Structural analysis of atovaquone-inhibited cytochrome bc1 complex reveals the molecular basis of antimalarial drug action. *Nat. Commun.* **5**, 4029 (2014).

81. van der Pluijm, R. W. et al. Triple artemisinin-based combination therapies versus artemisinin-based combination therapies for uncomplicated *Plasmodium falciparum* malaria: a multicentre, open-label, randomised clinical trial. *Lancet* **395**, 1345–1360 (2020).

Acknowledgements

Author contributions

J.T. and M.S. designed experiments. M.S. generated the data and J.T. analyzed the data and wrote the manuscript. S.N. performed sequencing data processing and Fourier transformation analysis. K.E.L., E.Q.

Competing interests

The authors declare no competing interests.

Ethics

The adult peripheral blood samples were collected under NUS-IRB (LH-18-054E) approved protocol.

Additional information

Supplementary information The online version contains supplementary material available at
https://doi.org/10.1038/s41467-024-51846-0.

Correspondence and requests for materials should be addressed to Jaishree Tripathi or Zbynek Bozdech.

Peer review information *Nature Communications* thanks Didier Menard and the other, anonymous, reviewer(s) for their contribution to the peer review of this work. A peer review file is available.

Reprints and permissions information is available at
http://www.nature.com/reprints

Publisher's note Springer Nature remains neutral with regard to jurisdictional claims in published maps and institutional affiliations.